

# Optimal site selection for Choutuppal geomagnetic observatory, based on geophysical evidences

Divyanshu Dwivedi<sup>1</sup>, Sneha Yadav<sup>2</sup>, Kusumita Arora<sup>1</sup>, Rakesh Murteli<sup>1</sup>, Alok Taori<sup>3</sup>

<sup>1</sup>Geomagnetism, CSIR-National Geophysical Research Institute, India

<sup>2</sup>Kurukshetra University, India

<sup>3</sup>National Remote Sensing Centre, India

Correspondence: Divyanshu Dwivedi; email id: [ddwivedigp@gmail.com](mailto:ddwivedigp@gmail.com)

Formatted: Font color: Auto

## Abstract

The phases of development ~~of the stages~~ of the Choutuppal magnetic observatory over last 15 years has enabled the effects of the natural environment like groundwater changes and lightning activity on the magnetic data to be evaluated. A ~~new-high~~ resolution survey ~~for-of~~ total field anomalies led to the construction of a 3D model of the shallow surface, and analysis of lightning data is carried out to understand the nature of the subsurface. Based on model from high resolution magnetic data and ~~Constrained by~~ conductivity depth slices from previous electrical resistivity tomography ERT and electrical vertical resistivity imaging EVRI surveys, the distribution of sandy regolith, saprolite, and granitic layers in the shallow subsurface ~~to be~~ delineated. The pattern of lightning strikes in a 10 km area around the observatory are correlated to modulations and disruptions in the magnetic data. This ~~The model analysis as a whole~~ provides information for selecting a location to install ~~the magnetic observatory~~ a secondary variometer room by taking into account topography, lightning effect, soil resistivity, low magnetic gradients anomaly, and distance from the recharge pond, which can produce continuous data of higher quality and consistency than at present.

**Keywords:** Choutuppal observatory, Magnetic anomaly, Spectral analysis, Lightning data

## 1. Introduction:

The Choutuppal (CPL) geo-electric observatory (Geographic coordinates: 78.920E, 17.290N; Geomagnetic coordinates: 149.24E, 7.47N) of CSIR-NGRI was established near Choutuppal town in the Nalgonda district, approximately 60 km southeast of Hyderabad city, Telangana state (Sanker Narayan, 1964). The region primarily comprises granite and gneissic formations. These rocks are part of the Peninsular Gneissic Complex, which is one of the oldest geological formations in India, dating back to the Archean era. The weathering of the granitic and gneissic rocks has led to the formation of red and lateritic soils. The granitic formation is encroached locally by discontinuities such as dikes or quartz reefs but these are not present on the site (Guihéneuf, Guihéneuf et al., 2014). The area around the CPL observatory mainly consists of alkali feldspar granite (Figure 1a). The regional geology of resistive granitic basement rocks, uniform soil cover, arid vegetation, and gentle topography for effective drainage of runoff water during rainy seasons were assessed to be suitable for geo-electric measurements (Sankar Narayan et al., 1967; Sarma et al., 1969). Below the surface, shallow drillings revealed: 1) A sandy regolith layer 0-2 m thick which is made up of sandy-clay of quartz grains, 2) A laminated saprolite layer of variable thickness of 10 -15 m derived from in-situ weathering of granite, 3) A 15-20 m thick layer of fissured granite, where weathered granite and some clay partially fill the fissures. The effective porosity of this layer is very low and mainly due to the fissure zones (Dewandel et al., 2006; 2012).

~~A topographic and magnetic survey was conducted in the region.~~ The geo-electric measurements at CPL were based on orthogonal 500 m electric dipoles and magnetic

Formatted: Font color: Auto

pulsations were measured with solid core induction coils. Hourly values of the magnetic variation and analysis of equatorial magnetic pulsations were reported from CPL (CSIR NGRI report, 1972). These hourly values are published in the Indian magnetic data volumes and uploaded to WDC Kyoto (Svensden et al., 1990). ~~Figure~~

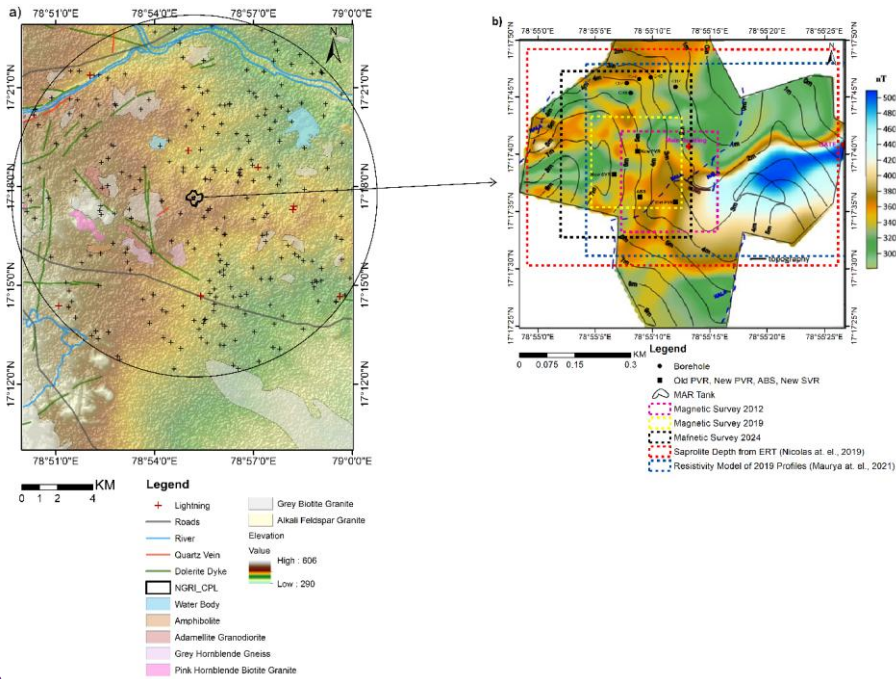
~~1b shows the 105-acre star-shaped campus of CSIR-NGRI in Choutuppal.~~ Figure 1b shows the 105-acre, star-shaped campus of CSIR-NGRI located in Choutuppal, along with the marked locations of the Primary Variometer (PVR) and Absolute (ABS) rooms.

One high magnetic anomaly is present at the eastern part of the campus. In the rest of the area, the total range is ~ -about 80 nT. The surface topography is least in the east and north and highest-higher is the west and southern part of the campus. Several shallow boreholes drilled in the northern end are used for hydrogeological studies in fractured hard rock terrains. These studies monitored the nature of the granitic basement rocks, local hydrogeology, and groundwater-managed aquifer recharge (MAR) within the CPL observatory, through a large, shallow lake in the eastern quadrant of the campus.

Geo-electric measurements on this campus were discontinued in , 1982—, but ~~Consequent to when~~ the Metro Rail project in the vicinity of the HYB magnetic observatory in Hyderabad appeared to threaten its existence in 2010, the Choutuppal campus was re-visited for re-location possibilities of HYB. This work ~~showcases~~ summarizes the different situations, which affect the operation of a low latitude magnetic observatory, some mitigation measures and some unanswered questions.

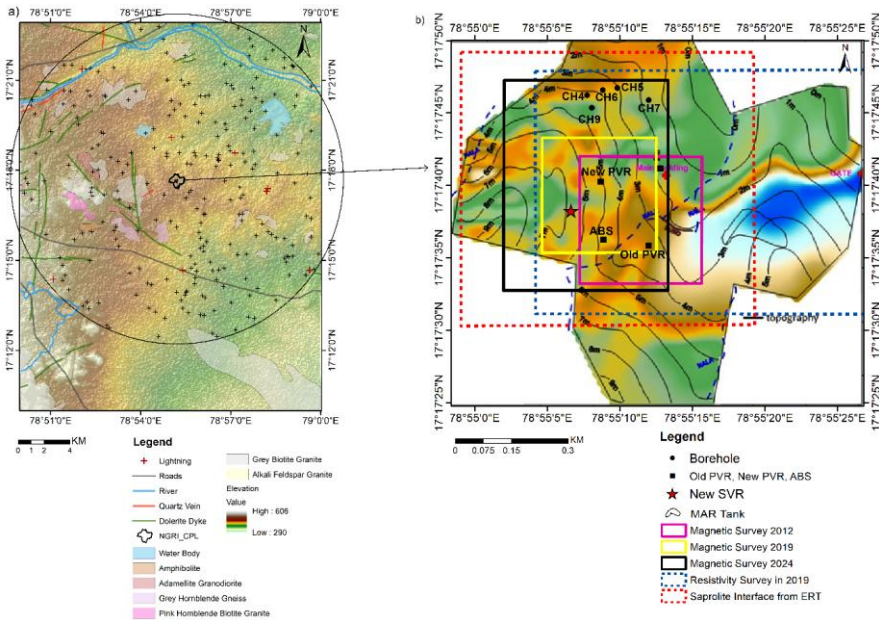
Formatted: Font color: Auto

Formatted: Not Highlight



Formatted: Font: (Default) Arial

Formatted: Centered



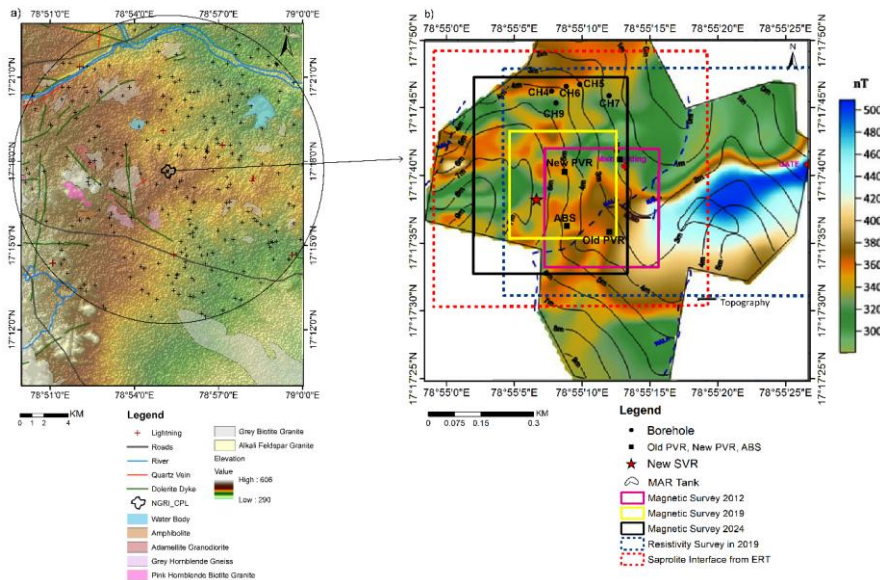


**Figure 1:** a) The geological map shows the area around the CSIR-NGRI- CPL observatory superimposed over topography. (SRTM Global 30 meter) situated on alkali feldspar granite, plus '+' symbols show lightning locations within a 10 km radius (circle mark) from January 2022 to August 2022 with maximum intensity 60480 amp, b) The magnetic anomaly map (after Sankehanar Narayan et al., 1967) is superimposed over the local elevation, with marked area of previous studies. The locations of the magnetic and electric surveys are marked by solid and dashed rectangles. PVR=Primary variometer room, NV=New Vault, ABS= Absolute room, SVR= Secondary variometer room, MAR = managed aquifer recharge.

## 2. First phase of CPL Magnetic Observatory:

### i) Survey of magnetic data gradients and building CPL Observatory

Prior to establishing the observatory buildings, a magnetic survey was conducted in November 2012 over an area of 200 m x 200 m with 20 m intervals, between the Main building-Building and the southern side of the campus, marked by pink dotted line rectangle in Figure 1b, which appeared to be have had the smallest anomalies gradients anomalies from as per the earlier survey. This area was sufficiently far away from the boundary of the campus to ensure that local activities outside the campus

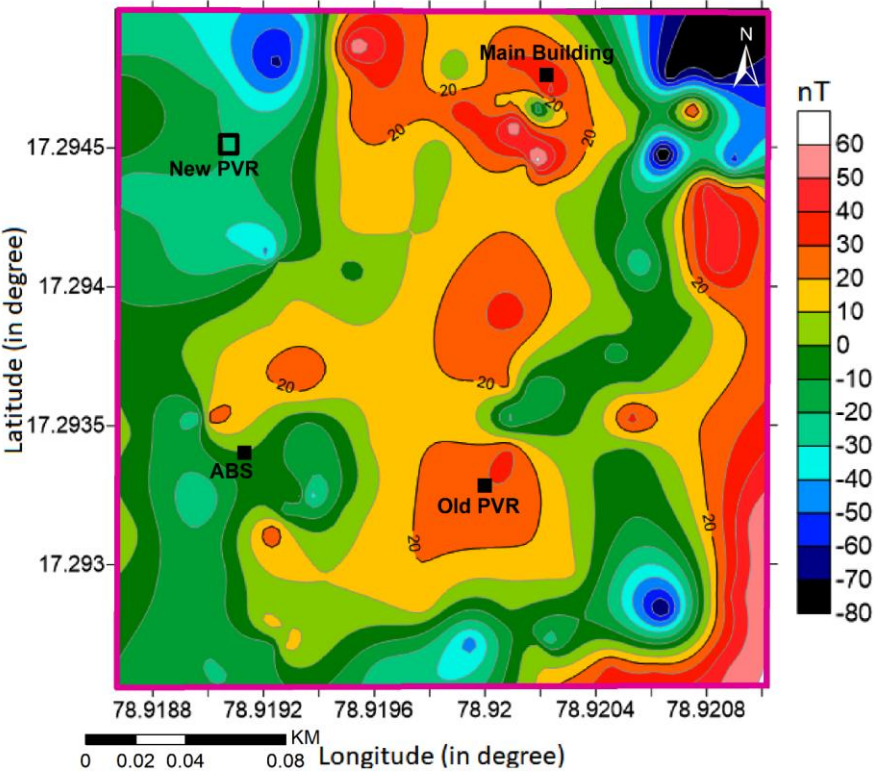
Formatted: Font color: Auto

Formatted: Strikethrough

Formatted: Font color: Auto

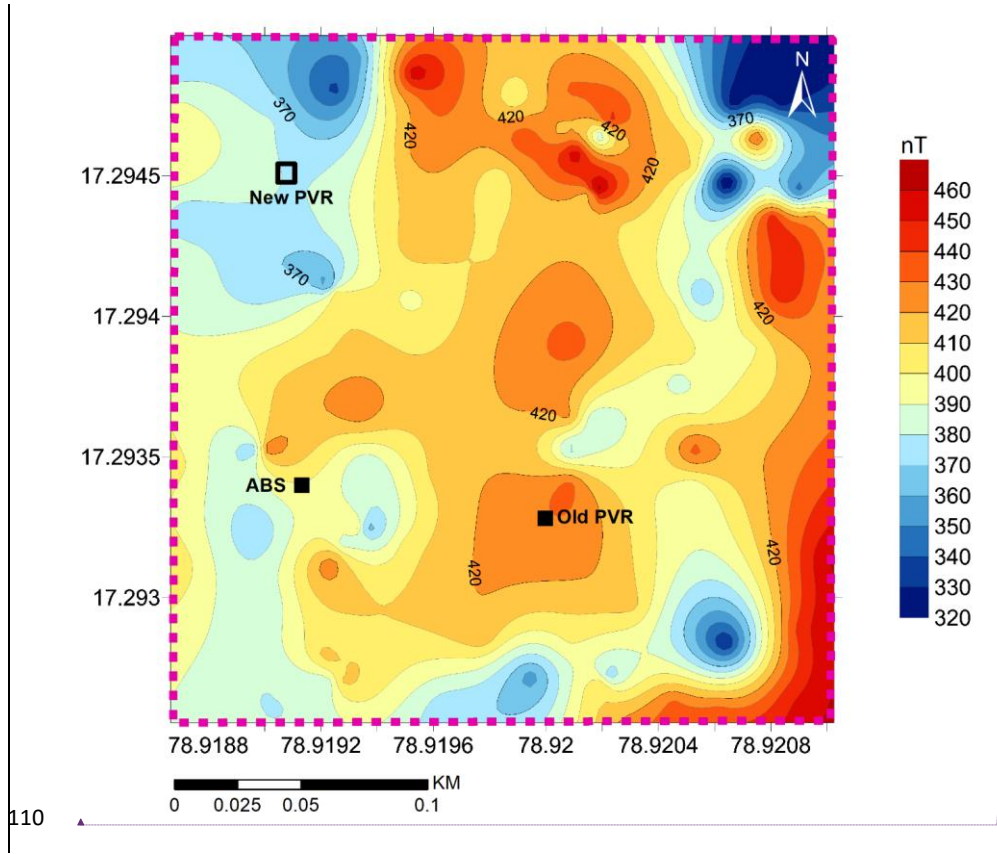
106 may not have significant contribution to the measurements. The total magnetic  
107 anomaly range (Figure 2) was ~ 150nT with changes in magnetic field within ~20 nT  
108 around proposed locations of the ~~old~~old PVR and ABS rooms.

**Formatted:** Font color: Auto



Formatted: Centered





Formatted: Font: (Default) Arial



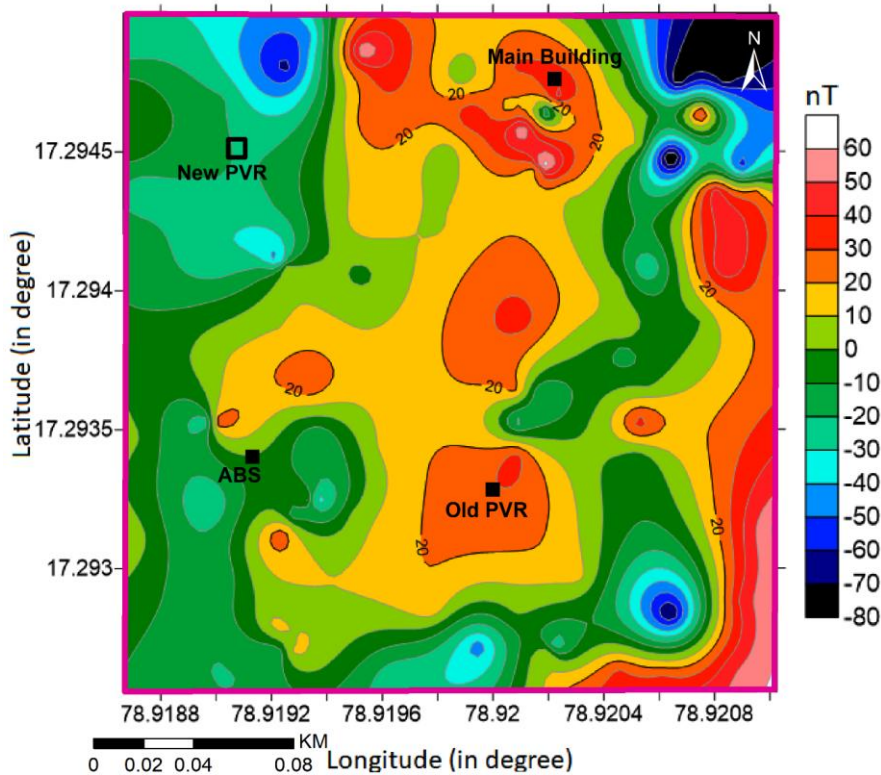


**Figure 2:** Magnetic anomaly plot of the survey region in 2012. Black box is the marked location for the New PVR, built in 2019-2020. Main Building to be marked on map

In this central location the surface topography ~~was moderately~~ low and a shallow water channel (nalla) ~~flowed~~ flows SE-NW through the area between the Old PVR and ABS. The ~~old~~ Old PVR construction (with double walled, 3.5 m underground vault) started in the June 2013 using non-magnetic sandstone. The ABS room was constructed on slightly elevated ground with two pillars inside and four pillars outside. In April 2014, the CPL observatory was commissioned, equipped with tri-axial fluxgate magnetometer and Zeiss single axis fluxgate theodolite for Declination-Inclination measurements. The XVII IAGA Observatory Workshop was held on ~~this~~ these

123 premises in October 2014 with 93 international participants from 33 countries. The  
124 definitive data from CPL is published at INTERMAGNET, 2015 onwards.

125

126 **ii) Hydrogeological Park and managed aquifer recharge:**

127 The region of CPL Observatory has a semi-arid climate with an average annual  
128 maximum temperatures ranging as 28°C - 45°C. The mean annual rainfall is around  
129 751 mm, which ranges from 2 mm in February to 171 mm in July. Water levels are  
130 highly variable depending on the monsoon and usually range between 2 and 26 m  
131 (meters below ground surface). Water level measurements at the northern part of  
132 the Choutuppal campus has been monitored since 1999 in two dozen boreholes, some  
133 of them are marked shown in Figure 1b, by the Indo-French Center for Groundwater  
134 Research (IFCGR) (Maréchal Mareschal et al, 2018) to study the hydrodynamic  
135 properties and associated hydrological processes in crystalline aquifers. As part of a  
136 governmental scheme of strengthening groundwater through recharge state-wise  
137 MAR projects, an infiltration basin was dug in Choutuppal (marked in black outline as  
138 MAR in Figure 1b) during in 2015 to meet the demands of farmers in the area  
139 facing water scarcity. The basin has dimensions of 120 m × 40 m, with a depth of about  
140 2 m, effectively removing the regolith layer and extending into the saprolite. The basin  
141 is mainly supplied by a canal which deviates-diverts water from the Musi River ,  
142 (Nicolas et al., 2019; Maurya et al., 2021) and was first filled in 2015. Nicolas et al  
143 (2019) has shown that intra-seasonal groundwater fluctuations have only moderate  
144 response to rainfall patterns, which could be due to usage trends as well as hydraulic  
145 permittivity parameters. After the MAR basin filling, groundwater levels rose by 6 m in  
146 one year. Figure 3a shows the water level changes of five boreholes (CH5, CH4, CH6,  
147 CH7, and CH9) before and after monsoon from 2011 to 2023 with a data gap during

Formatted: Font color: Auto

Formatted: Font color: Auto

Formatted: Font color: Auto

Formatted: Font color: Auto

Formatted: Font color: Auto

Field Code Changed

Formatted: Font color: Auto

148 2021-22. While it is clear that most of the time water level lies at intermediate depth of  
149 ~ 10 to 30 m, individually, CH5 and CH7 show the least seasonal fluctuations over the  
150 years, CH6, CH4 and CH9 show variations of 20 m or more; possibly very local fracture  
151 properties facilitate vertical flow of ~~downward seepage of water preferentially~~. Starting  
152 from April 2017, the water levels in the boreholes rose significantly, coming almost to  
153 surface in September 2017 and reducing a little by July 2018. In December 2023, the  
154 water levels recorded are nearly similar to that of September 2017. It can be inferred  
155 that sustained water in the MAR basin has allowed the shallow aquifers to be  
156 permanently recharged. In September 2017, the rainfall of the monsoon combined  
157 with prevalent saturated condition led to the flooding of the ~~magnetometer room~~Old  
158 PVR vault. ~~The vault of the PVR rose nearly to surface and damaged the fluxgate~~  
159 ~~magnetometer and electronics~~ (Figure 3**cb**). The water level receded by a few metre  
160 the following summer but did not fall to earlier levels. While this was good news for  
161 recharge, the Old PVR was ~~made now~~ unusable.

Formatted: Font color: Auto

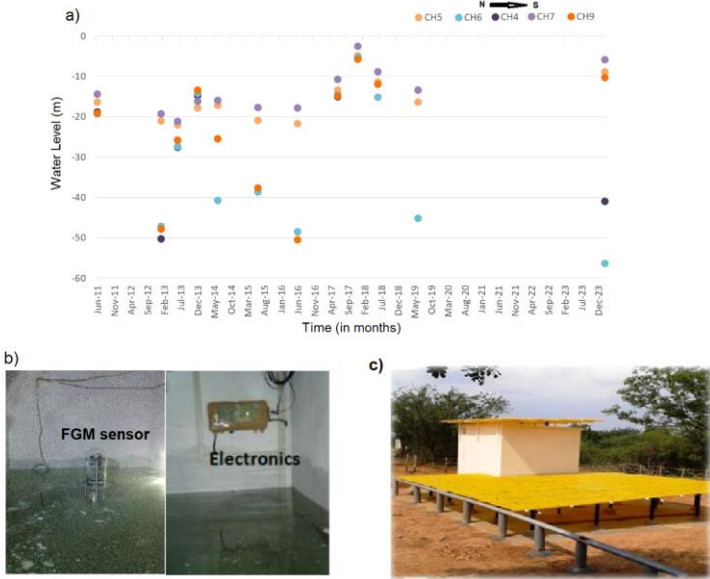
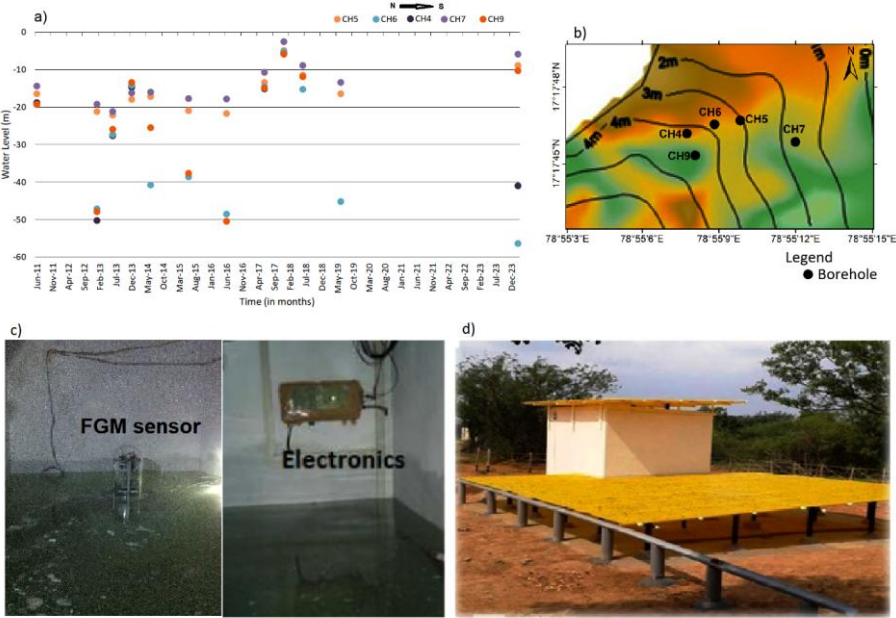


**Figure 3:** a) Fluctuations of water level in a few boreholes in the north of Choutuppal campus, [b\) location of boreholes in the map](#), [c\) the submerged vault](#)

in September 2017, ~~de~~) the outside view of the old PVR. ~~Include an enlarged pic of the boreholes in map~~

### 3. Second phase of CPL Magnetic Observatory:

#### i) Survey and commissioning of new PVR

With the need for a new variometer building, a fresh survey was conducted in May 2019 using GSM19 Overhauser magnetometers, marked by ~~the yellow dashed box~~rectangle in Figure 1b. This area was some tens of meter west of the earlier survey location, still central to the campus, on ground which is about 2-3 m higher, ~~which could avoid the shallow groundwater conditions~~. This total field magnetic survey was carried out during six ~~days~~ (geomagnetic quiet days) in May 2019 over a 240\_X\_240 square meter area with 10 m spacing. The magnetic anomaly of the region shows total amplitude variation of ~300nT (Figure 4a) with ~10nT anomaly north of the ABS room; the proposed location is marked as New PVR in Figure 4a. This time a raised building with double walls and double roof was constructed of non-magnetic limestone to ensure no groundwater incursion issues for the foreseeable future (Figure 4b). The New PVR was commissioned in January 2021.

Formatted: Font color: Auto

Formatted: Font color: Auto

Formatted: Font color: Auto

Formatted: Font color: Auto

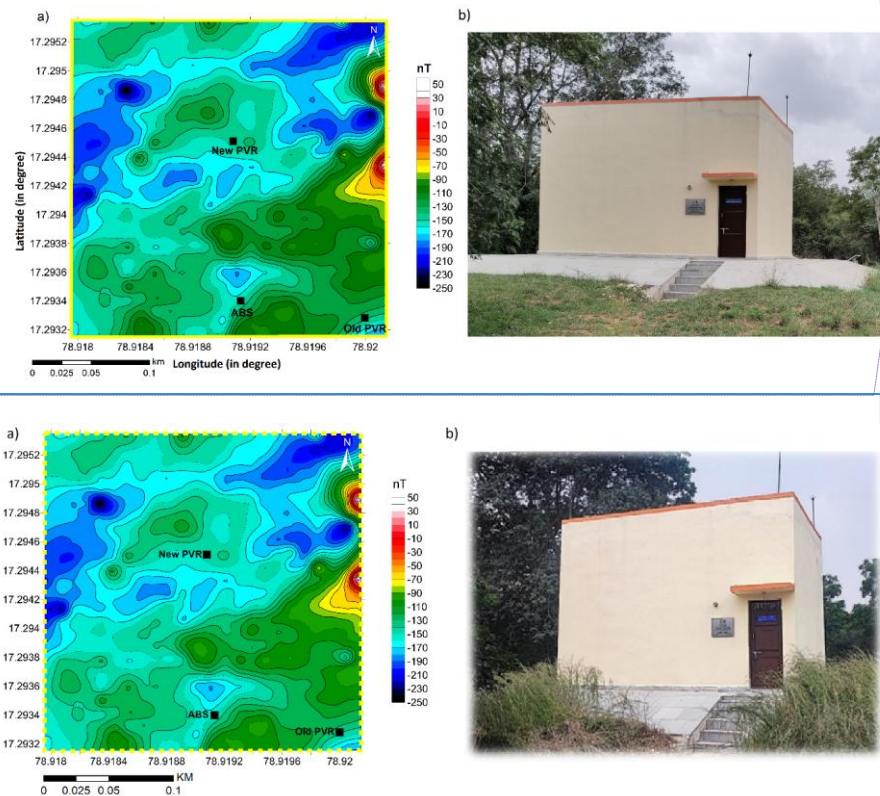


**Figure 4:** a) Magnetic anomaly plot of the survey region in 2019, b) New PVR building inaugurated in January 2021.

Recurrent malfunctions of the electronics (2-3 times a month) of the digital fluxgate magnetometer (DFM) recording system electronics were noticed in second half of 2021 and 2022, a new phenomenon. After rounds of thorough inspections, These incidences were later correlated with it was suspected that lightning activity in the vicinity of the Choutuppal campus was causing the damage inspite of installation of 6 lightning arrester rods and 4 earthing pits. Being an open ground with no tall obstructions, the lightning activity in this area was found to be more frequent than



around HYB observatory in Hyderabad. ~~Strengthening of~~ The earthing pits and lightning arrester system were strengthened further but only marginally countered the effects on the electronics.

**ii) Lightning activity patterns around CPL Observatory and effects on data**

ISRO-National Remote Sensing Center (NRSC) has a network of 46 radio frequency27-VLF lightning detection sensors, covering the southern-entire part of the India country (shown in Figure 5a). The Lightning detection sensor network monitors the cloud to ground lightning occurrences by virtue of emitted waves in the 5 Hz - 30 MHz range and geolocation is calculated using the time of arrival method. The detection range is upto 800 km with more than 98% confidence within 300 km range, with 50% overlap to maintain high geo-location accuracy of lightning occurrences ~~The detection range is upto 800 km with more than 98% confidence within 300 km range, with 50% overlap to maintain high geo-location accuracy on the recent past which may be due to the induced current generated in the subsurface~~ (Taori et al., 2022; 2023).

We have examined the lightning data in a radius of 10 km around CPL observatory, marked as + in Figure 1a. Figure 5b shows the shows the occurrence frequency of lightning over the months from January to August 2022; + symbols denote the instances when the lightning caused damage in the fluxgate electronics. Figure 5b shows that substantial lower intensity lightning activities are recorded during January, April, May and June. Surprisingly July had no lightning in the area in 2022, in August, the higher intensity lightning were more numerous. Two instances of failure of the instrument electronics occurred during the higher intensity lightning of April and

Formatted: Font color: Auto

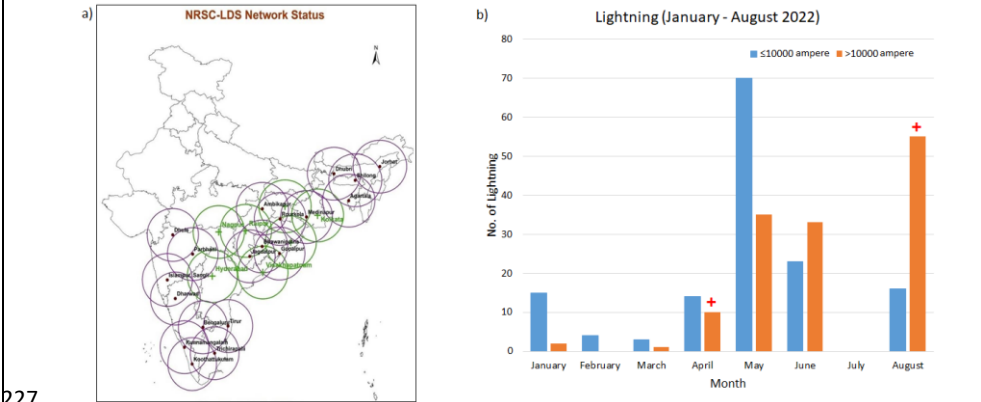
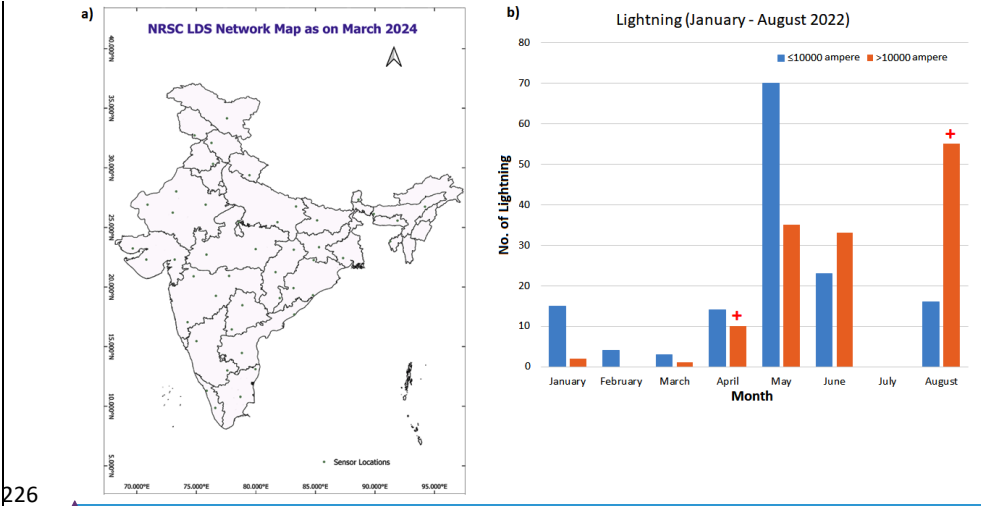
Formatted: Font color: Auto

Formatted: Font color: Auto

Formatted: Font color: Auto

Formatted: Font color: Auto

224 August, whereas a disturbance of May was associated with lower amplitude lightning,  
225 discussed in next section.

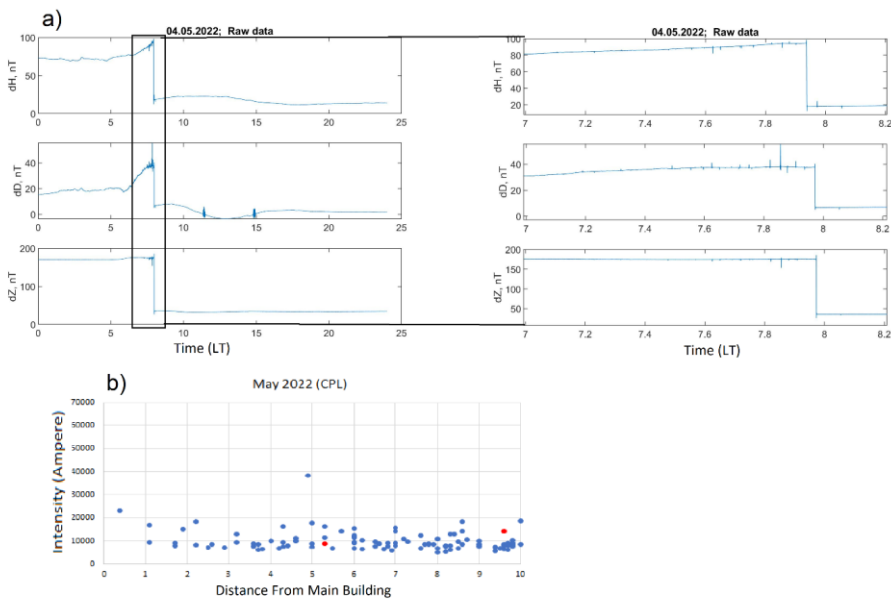


228 **Figure 5: a)** Map of lightning sensors [in India](#), **b)** Distribution of low and high intensity  
230 lightning occurrences during January to August 2022.

233 Examination of the H ([horizontal](#)), D ([declination](#)), and Z ([vertical](#)) components of 1-  
234 sec data in LT ([local time](#)) for 04<sup>th</sup> May, 2022 data from the new PVR shows continuous  
235 spikes from 7- 8.2 LT in all the components, followed by a shift of ~ 70, 20 and 150 nT

236 in H, D and Z respectively (Figure 6a). After rebooting the instrument, the data came  
237 back to its normal range. Comparison with lightning data established that this  
238 disturbance was due to lightning effect (correlated red mark). It is noticed that at the  
239 time of 7.94 LT hour there was shift in the data which correlate with the lightening  
240 intensity of 8879 amps and 14243 amps at the same time (Lightning data from NRSC)  
241 which strike the ground within 10 km radius of CPL campus.

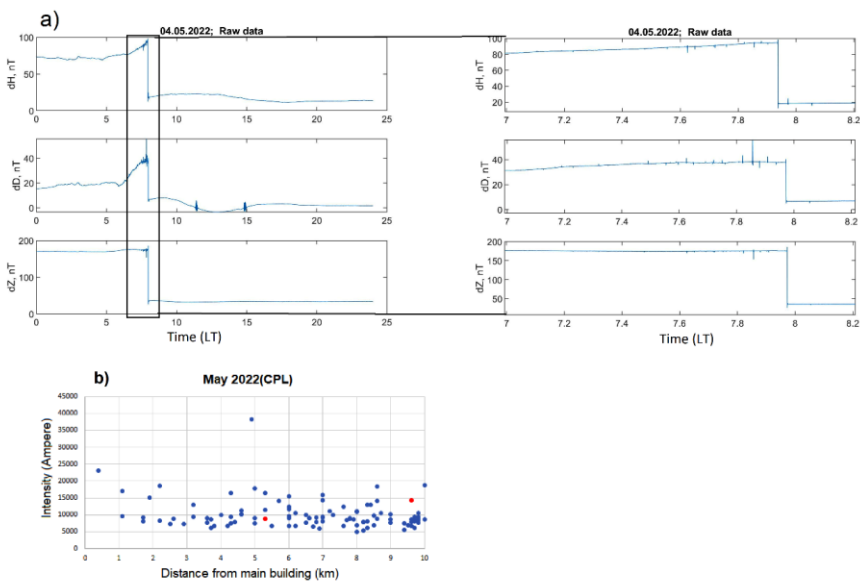
**Formatted:** Font color: Auto



Formatted: Font: (Default) Arial, Bold

Formatted: Centered

242



243

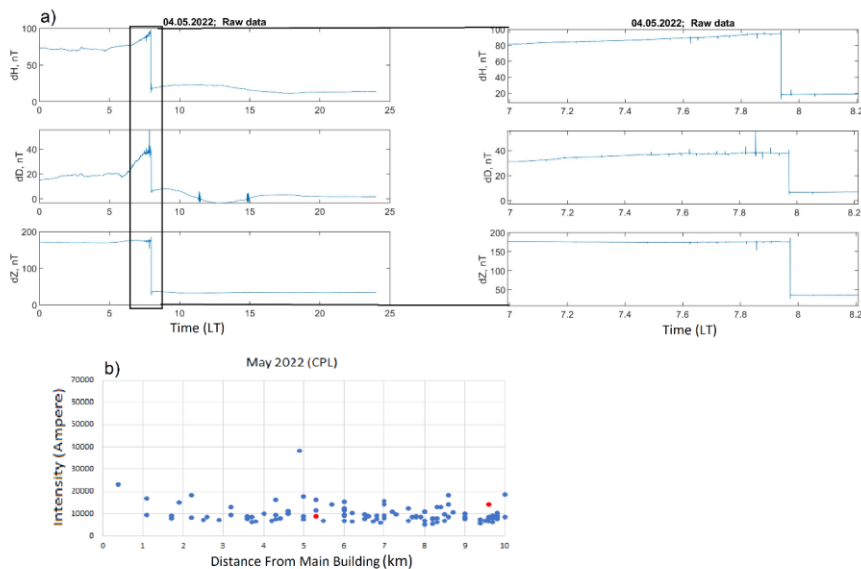
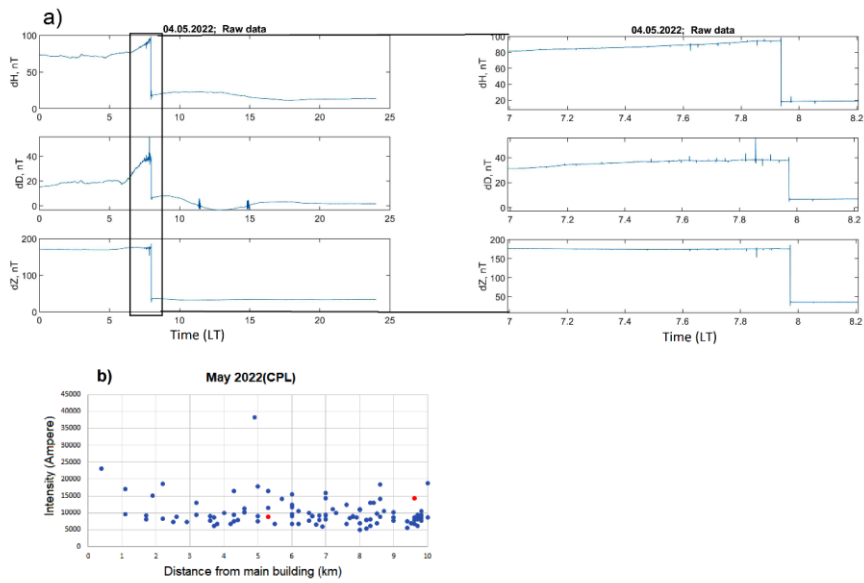


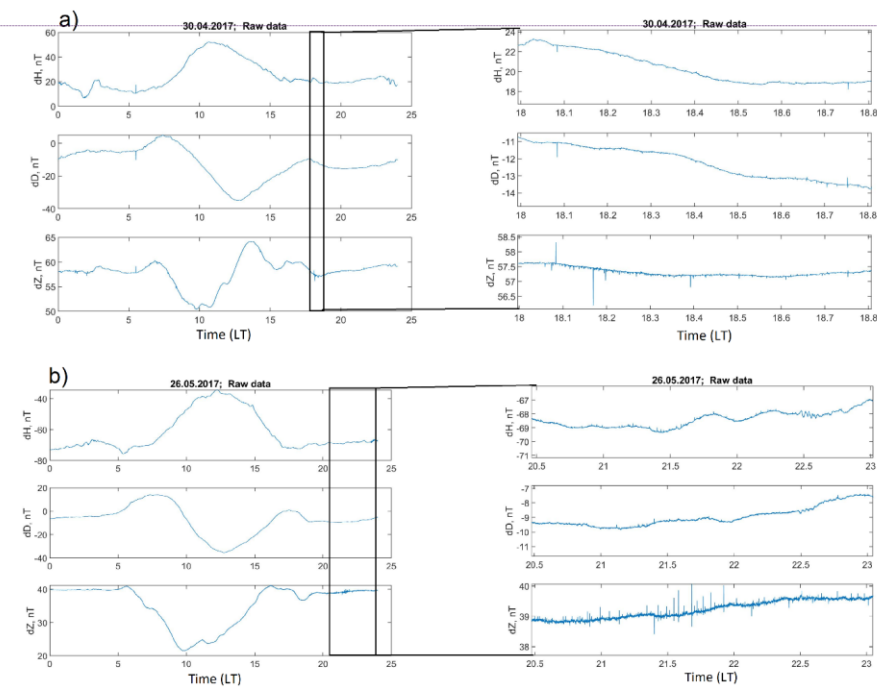
**Figure 6:** Raw data (H, D, Z component) plot for a) 04<sup>th</sup> May, 2022 at the new PVR, b) plot of lightning intensity ([in ampere](#)) with distance (in km) from main building.

Further, we examined the H, D, Z components of 1-sec data in LT or the 30<sup>th</sup> April and 26<sup>th</sup> May, 2017 data from the [Qeld PVR](#), on days which had some weather activities. From the data, it is clear that there were no shifts in the data, but some continuous spikes were observed from 18.0 -18.8 LT (Figure 7). The spikes are more prominent in the Z component ( $>0.5\text{nT}$ ). Though lighting data was not available in this duration, the general conditions lead us to believe that these minor signatures were lightning induced.



Formatted: Font: (Default) Arial

Formatted: Centered



Formatted: Font: (Default) Arial, Bold

Formatted: Line spacing: single



**Figure 7:** Raw data (H, D, Z component) plot for a) 30<sup>th</sup> April, 2017, b) 26<sup>th</sup> May, 2017 at the old PVR.

**Table 1** provides examples of the amplitudes of the disturbances recorded in data vis-à-vis the light intensities and distance from the recording system

<u>Date</u>	<u>Time (LT)</u>	<u>H</u>	<u>D</u>	<u>Z</u>	<u>Lightning amplitude (ampere)</u>	<u>Distance (km)</u>	<u>Remark</u>
15-04-2022	23.2 - 24.00	0.1nT	0.2nT	1nT	20968	5.5	GSM90 stopped recording & spikes in HDZ
04-05-2022	7.0 - 8.2	70nT	20nT	150nT	8879, 14243	5.3, 10	Shift in data(HDZ)
29-08-2022	=	=	=	=	37387, 24329, 21210, 8553	3.9, 5.5, 9.2, 10	DFM Stopped recording
30-04-2017	18.0 - 18.8	0.8nT	1nT	1.2nT	=	=	Spikes in HDZ
26-05-2017	20.5 - 23.0	0.2nT	0.2nT	1nT	=	=	Spikes in HDZ

Formatted: Font: Bold

Formatted: Line spacing: single

Formatted: Line spacing: single

<u>Date</u>	<u>Time (LT)</u>	<u>H</u>	<u>D</u>	<u>Z</u>	<u>Lightning amplitude (ampere)</u>	<u>Distance (km)</u>	<u>Remark</u>
15-04-2022	23.2 - 24.00	0.1nT	0.2nT	1nT	20968	5.5	GSM90 stopped recording & spikes in HDZ
04-05-2022	7.0 - 8.2	70nT	20nT	150nT	8879, 14243	5.3, 10	Shift in data(HDZ)
29-08-2022	=	=	=	=	37387, 24329, 21210, 8553	3.9, 5.5, 9.2, 10	DFM Stopped recording
30-04-2017	18.0 - 18.8	0.8nT	1nT	1.2nT	=	=	Spikes in HDZ
26-05-2017	20.5 - 23.0	0.2nT	0.2nT	1nT	=	=	Spikes in HDZ

It ~~can inferred~~was suspected that ~~because the location of the~~ new PVR ~~is constructed~~constructed on the surface and the cables ~~as well as fact that the pillars and infrastructure were installed~~were laid in the surface layer, instead of ~~the 3-4 m deeper~~ vault configuration as in the one which was flooded, ~~has amplified~~ the effects of lightning activity on the data has been amplified. Given the fact that in future years more uncertainty and swings in climatic parameters are anticipated due to effects of climate change, it was deemed necessary to conduct further studies to find a location based on optimal ranges of a variety of parameters like topography, distance from MAR lake, the configuration of near surface regolith and saprolite layers along with groundwater conditions.

#### 4. New search for optimal location

Higher ground away from the MAR basin can be found toward the western side of the campus. In order to evaluate its suitability as a new long term location for continuous magnetic measurements, This study aims to delineate the sub-surface structures using the high-resolution magnetic data ~~in combination with~~constrained by resistivity information conducted through Electrical Resistivity Tomography (ERT) and Electrical Vector Resistivity Imaging (EVRI) measurements at the Choutuppal campus and surrounding areas during 2016-2017. The magnetic method can be sensitive to presence of near surface variations and produce a model of these layers as well as in locating faults, folds, shear zones, delineating geological structures, and groundwater contamination studies (Reynolds, 1997; Hinze et al., 2013; Kumar et al., 2018; Dwivedi and Chamoli, 2021, 2022). ~~Finally, w~~We try to find out a suitable location ~~called for a~~ new SVR (secondary variometer room) where effects of lightning and groundwater level changes can be minimum in the medium-to-long term.

**i) 2024 survey**

A 1-sec total magnetic field survey was conducted during February 2024 (4 days) at 10 m sampling intervals as same done in 2019 survey. The data of 2019 and 2024 were combined, thus covering a total of ~ 400x320 square meters. The diurnal and International Geomagnetic Reference Field (IGRF 14) corrections are applied to the F data, so that the residuals reflect only the local crustal contributions. Finally, we applied the kriging interpolation method to generate the grid and produce the magnetic anomaly of this area (Figure 8a). Further, this was converted by a 'reduced to equator' computation to remove ambiguities in location of causative sources of magnetic anomalies, at low and high latitudes. In this study, we chose the values of Delineation=0°, and Inclination=24° and estimate the [reduction to equator \(RTE\)](#) generated magnetic anomaly map of the study region. The RTE filtered map centres anomalies over their sources and removes the asymmetry of the magnetic anomaly due to nonzero magnetic inclination and helps in magnetic data interpretation (Figure 8b).

Formatted: Font color: Auto

Formatted: Font color: Auto

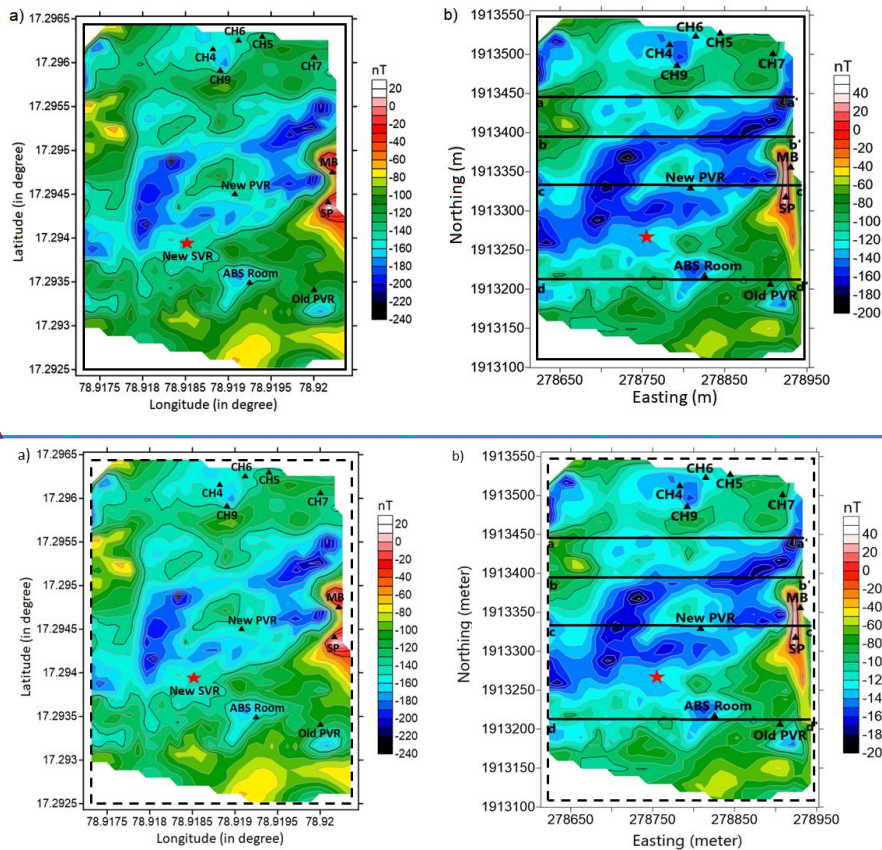


**Figure 8: a)** The magnetic anomaly of the study area. (MB=main building, SP= solar panel, CH= bore well channels, ABS= absolute, PVR= primary variometer room, SVR= secondary variometer room). Red star mark shows the proposed New SVR in the region, **b)** the magnetic anomaly after reduction to equator of the study area. The aa', bb', cc' and dd' shows four magnetic profiles modelled.

The RTE magnetic anomaly shows a variation of  $\sim 260$  nT in the region. The low anomaly is dominant in the central part followed by the high anomaly near the main building and solar panel. The new PVR lies in the low anomaly region where the three-axis flux magnetometer is installed to record 1-sec H, D, and Z component data of Earth's magnetic field. The ABS room [location](#) is set up in the low anomaly zone to

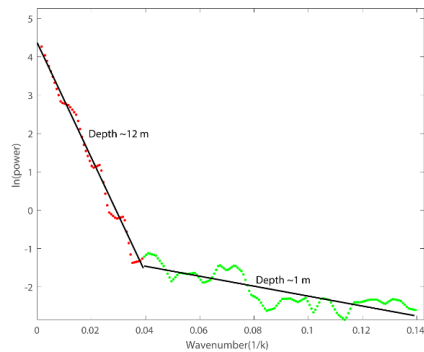
measure the Delineation-Inclination using the Mag-01 DI-fluxgate magnetometer mounted on theodolite.

We have considered four profiles aa', bb, cc', and dd' along EW in the RTE magnetic anomaly map to characterise the subsurface susceptibility model (Figure 8b). The magnetic data shows its importance in characterizing the shallow sub-surface structures, which would be further beneficial for the selection of new location to install magnetic observatory in the campus. The lightning data is considered from the National Remote Sensing Centre (NRSC), Hyderabad, India, to investigate the failure of the DFM (digital fluxgate magnetometer) -electronics during the lightning strike. The high-resolution topography data is obtained from the Shuttle Radar Topography Mission (SRTM) Global 30 (<https://earthexplorer.usgs.gov/>) to plot the elevation of the region.

The ERT surveys for different profiles (AA', DD', EE', FF' and GG') were carried out using Wenner and Schlumberger arrays with 48 electrodes in the campus. The profiles AA', DD', EE' with 5 m unit electrode spacing achieved a maximum length of 360 m whereas FF' and GG' covers 240 m (Maurya et al, 2021). The vertical cross section along these profiles and a horizontal depth slice at a depth of 30 m below ground level derived from 3D model reflect few linear conductive features and surficial resistivity heterogeneities (Figure 13a). The details about these surveys and results can be seen in Maurya et al., (2021).

## ii) Analysis of subsurface source and depths

The fast Fourier transform (FFT), a robust technique is used by several researchers to calculate the mean depth of layered interfaces of the potential field datasets (Chamoli et al., 2011, 2023; Dwivedi et al., 2019). The power spectrum analysis gives the average depth of the sources with an error limit of 10% (Mishra and Pederson, 1982). The 2D radially averaged power spectrum of the RTE magnetic anomaly data shows two linear slope segments corresponding to the average depth of two interfaces around  $12 \pm 1.2$  m and  $1 \pm 0.1$  m (Figure 9).





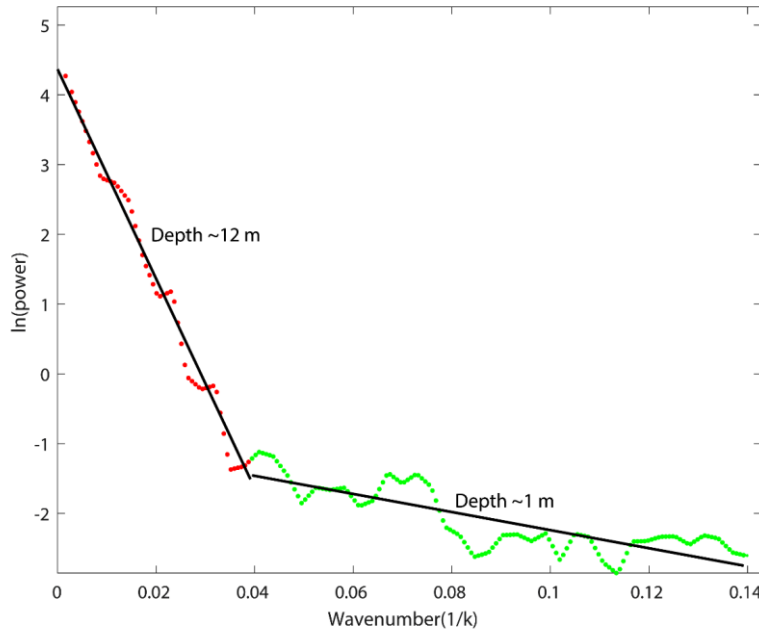


**Figure 9:** Radially averaged power spectrum of the RTE magnetic anomaly. Different layer segment give an average depth of layered interfaces.

The tilt depth is an effective method in characterizing the location of source edge as well as magnetic source depth using the tilt angle (TDR) approach (Salem et al., 2007). First, the TDR is described by the following equation (Miller and Singh, 1994).

$$\theta = \tan^{-1} \left[ \frac{\frac{\partial M}{\partial z}}{\sqrt{\left(\frac{\partial M}{\partial x}\right)^2 + \left(\frac{\partial M}{\partial y}\right)^2}} \right] \quad (1)$$

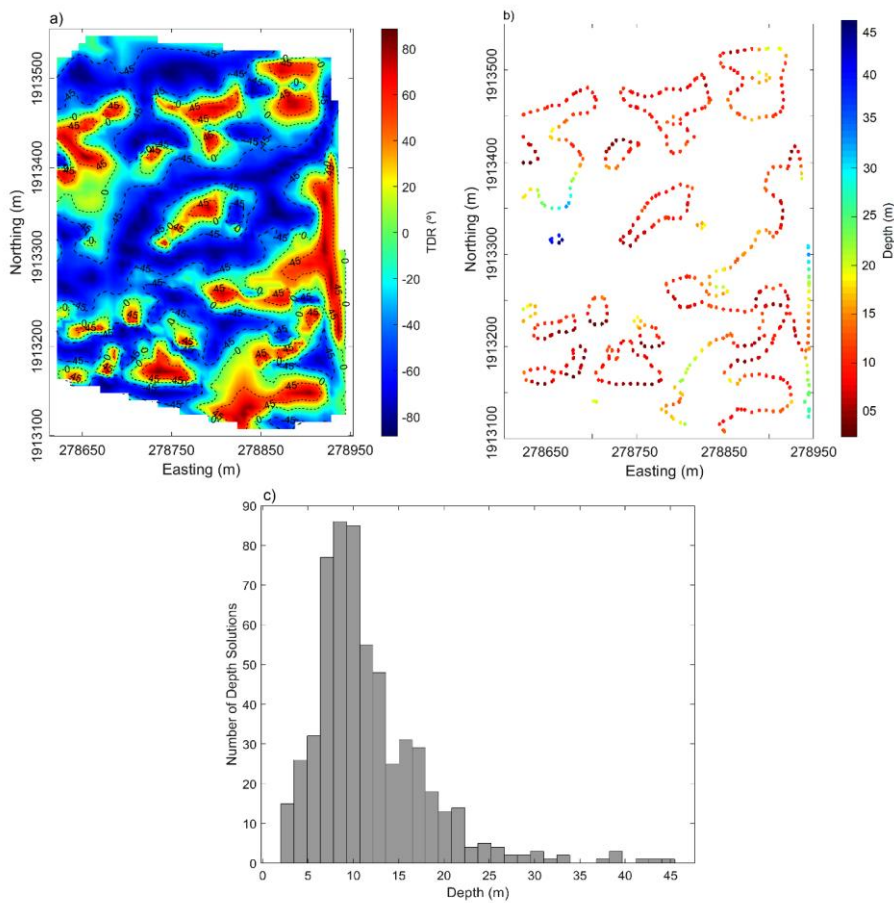
where  $\frac{\partial M}{\partial x}$ ,  $\frac{\partial M}{\partial y}$ ,  $\frac{\partial M}{\partial z}$  are the first derivative of the magnetic field M in the x, y and z directions. The zero contour ( $\theta = 0^\circ$ ) demarcates the spatial location of magnetic source and tilt amplitudes restrict in the range of  $+90^\circ$  to  $-90^\circ$ . Salem et al., (2007)

introduced the tilt depth technique using the relationship among tilt angle ( $\theta$ ), depth ( $Z_c$ ), horizontal location ( $h$ ) of a contact as:

$$\theta = \tan^{-1} \left[ \frac{h}{Z_c} \right] \quad (2)$$

In the equation 2, the contact location ( $h=0$ ) lies to the zero values of the contour and depth relates to the horizontal distance between the  $0^\circ$  and  $\pm 45^\circ$  contour in the TDR map. We apply the technique to generate the tilt angle (TDR), tilt depth solution and histogram plot on the magnetic gridded data. Figure 10 presents the TDR map with displaying of contours of  $-45^\circ$ ,  $0^\circ$ ,  $+45^\circ$  (dashed black lines). The TDR shows the short wavelength anomalies and closely spaced contours that corresponds to shallow sub surface sources. The zero contour values of the TDR show the location of the source whereas the half of the distance between  $\pm 45^\circ$  contours demarcates depth of the sources. It can be seen that distance between  $0^\circ$  and  $+45^\circ$  is demarcated by relative closeness over the shallow sources and wide expanses over the deeper sources.

Formatted: Font color: Auto



Formatted: Font: (Default) Arial

Formatted: Centered

Formatted: Line spacing: single

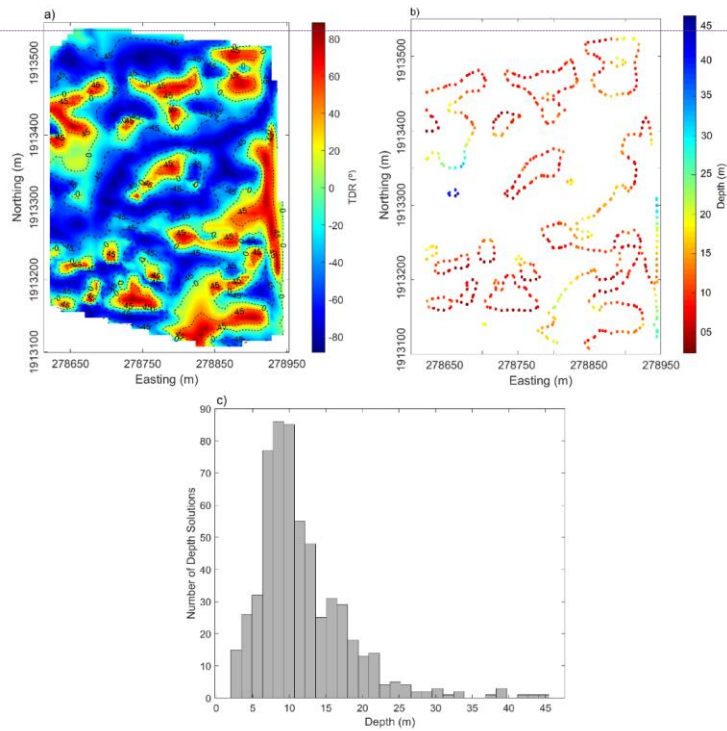


**Figure 10:** a) The tilt angle plot, b) The tilt depth solutions, c) the tilt depth solution histogram plot of the RTE magnetic anomaly.

The tilt depth solutions of the RTE magnetic anomaly data with depth variation from ~ 2 m to 45 m. Most of the sources lie in shallow depth ~ 2 to 20 m and extended in one direction. The histogram plot shows the variation between number of depth solution and depth (Figure 10c). It is clear from the plot that number of depth solution are maximum in the depth range of ~ 2 m to 20 m which corresponds to shallow source in the sub surface.

### iii) Magnetic data inversion and forward models

We invert the RTE magnetic anomaly to estimate the depth variation of the interface with strong susceptibility contrast. We use the method of Parker (1973) which works in the Fourier domain to estimate the depth variation of an undulated interface. The depth of interface can be computed from the magnetic anomaly due to an uneven, uniform magnetized layer by inversion procedure. The method is improved by incorporating high cut filter to ensure the convergence of series and to avoid instability at high wavenumber (Pham et al., 2020). Based on the power spectrum characteristics, we have chosen the cut-off wavenumber between 0.038-0.13  $\text{m}^{-1}$  to remove the high frequencies. The resultant map shows that this interface is deepest in the centre of the survey area and shallowest towards the edges; then present PVR and the ABS Room are in the zones where this interface is deep, whereas the old PVR, which was flooded was in the zone of shallow interface (Figure 11a). The calculated depth is inferred as the saprolite layer, which varies from ~ 12 to 16 m with a mean depth of ~14 m. Figure 11b shows the variation of the root mean square (RMS) error against the iteration number. In this case, the inversion process performed 175 iterations, and the RMS error between two successive approximations was reduced from 0.0680 m to  $9.9584 \times 10^{-5}$  m.

Formatted: Font color: Auto

Formatted: Font color: Auto

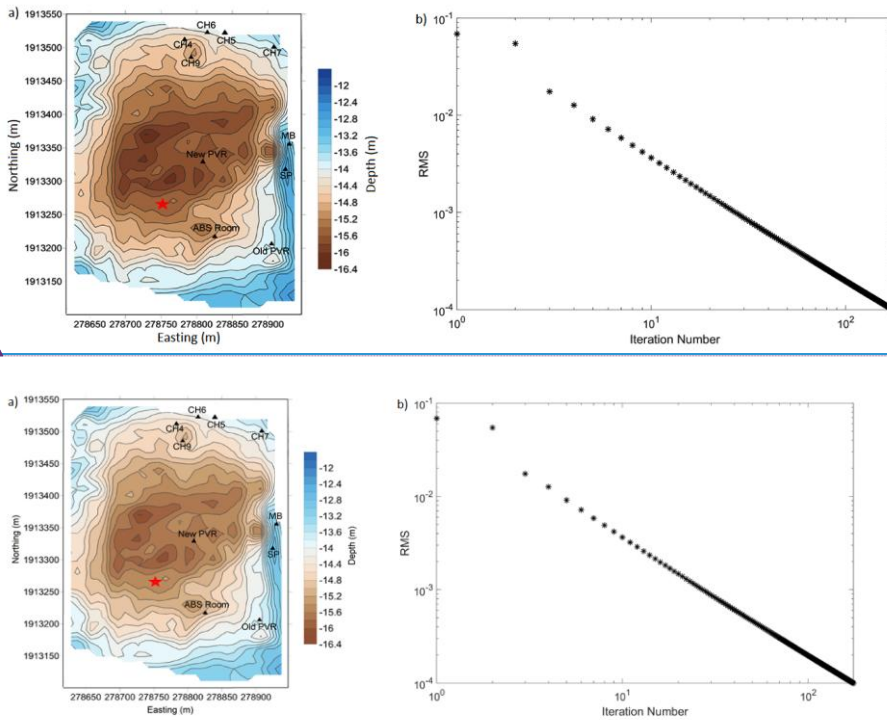
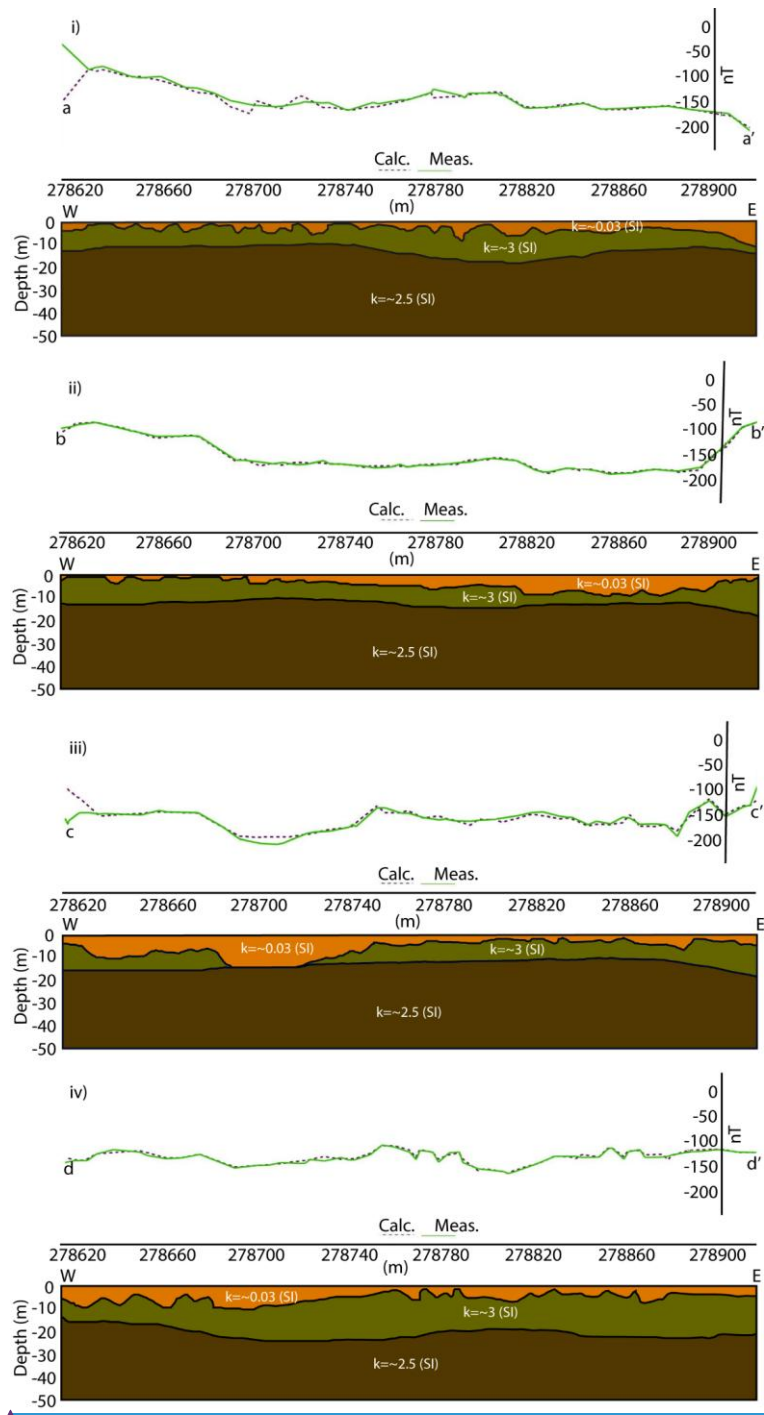


**Figure 11:** a) The depth variation of the saprolite interface derived from the inversion of the RTE magnetic anomaly after removing the high frequency component, b) variation of RMS error against the iteration number.

Further, we model the RTE derived magnetic anomaly data along four profiles aa', bb', cc', and dd' (Figure 8b) to delineate the details of the sub-surface structures. The forward modelling along these profiles is carried out using the IGMAS+ software, a tool for forward and inverse modelling of potential field datasets (Anikiev et al., 2023). The total length of these profiles are ~310 m which show the depth variations up to 50 m from the surface (Figure 12a–12d). The 2D models along these profiles explain the presence of three layered structures from the surface up to a depth of 50 m as: sandy regolith (~0.3 susceptibility in SI), saprolite (~3 susceptibility in SI), and fissured granite (~2.5 susceptibility in SI). The average susceptibility value for sandy regolith



508 layer is measured in the field using KT-10 magnetic susceptibility meter whereas  
509 others are referenced from Telford et al., (1990). The saprolite interface is incorporated  
510 in the models based on previous results of ERT data (Nicolas et al., 2019). The  
511 average thickness of the sandy regolith layer is ~3 m whereas the saprolite layer is ~  
512 10 m in the models. Both the saprolite and regolith layers show undulations in the all  
513 models.



Formatted: Font: (Default) Arial

Formatted: Centered

515

516

517

518

519

520

521

522

523

524

525

526

527

528

529

530

531

532

533

534

535

536

537

538

539

540

541

542

543

544

545

546

547

548

549

550

551

552

553

554

555

556

557

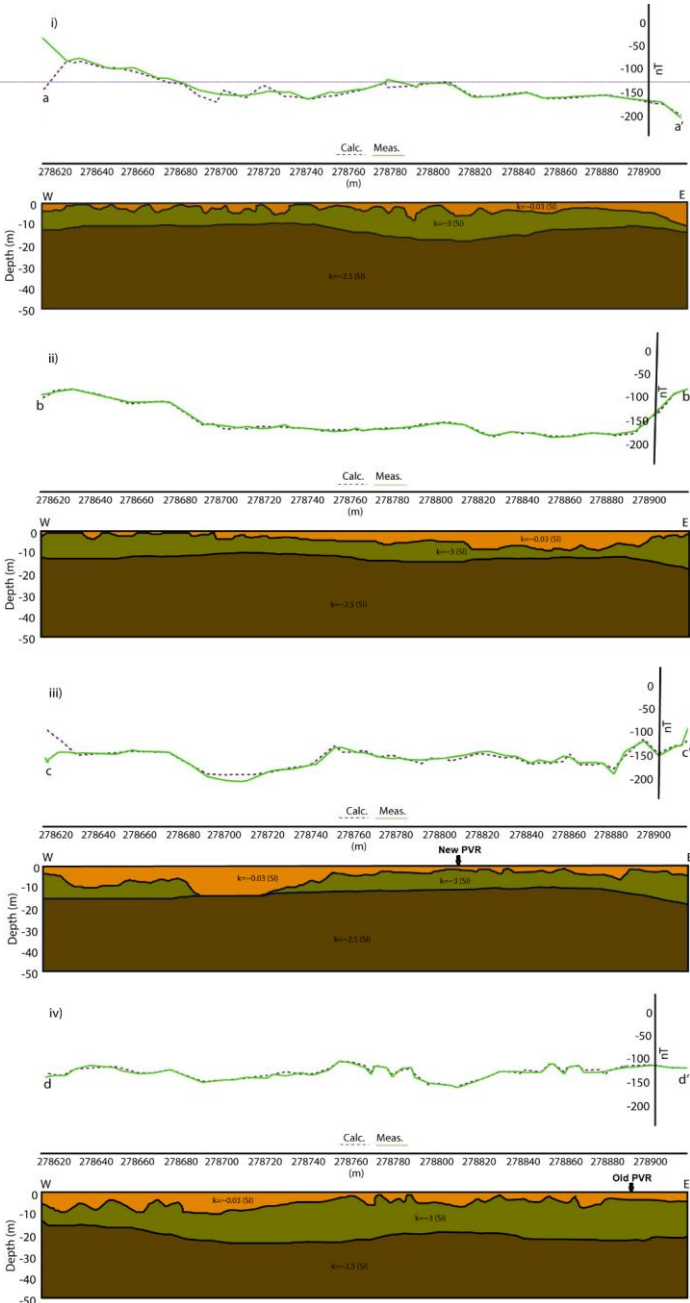
558

559

560

561

562



Formatted: Centered, Line spacing: Double

Formatted: Font: (Default) Arial, Bold

Formatted: Line spacing: single

**Figure 12:** Magnetic data modelling across the profiles i) aa', ii) bb', iii) cc' and iv) dd' incorporating constrain from power spectrum, and past ERT studies. Top, middle and bottom layers in the models are sandy regolith, saprolite and granitic basements. The marked arrows show the location of New and Old PVR in profile cc' and dd'.

#### iv) Correlation with conductivity data/information

The cc' magnetic profile is close to the vertical resistive cross-section along AA' of Maurya et al., (2021) where resistivity increases from surface to depth (Figure 13a).

The old surface and apparent resistivity data of the region is digitized from the Sanker Narayan et al., (1967) and overlaid over the topography (Figure 13b, 13c). The apparent resistivity shows lateral varying high resistivity outwards and vice-versa inside the Choutuppal campus (Figure 13c). This indicates that conductivity decreases outward, highlighting the presence of conductive soil layers within the campus. ~~This means that conductivity decreases away and reflects the presence of conductive soil inside the campus.~~

The calculated saprolite depth by inverting magnetic data at different locations are ~ 15.5 m (new PVR), ~ 15 m (ABS Room and CH9), ~ 13 m (MB and SP), ~14 m (old PVR, CH5, CH6, CH7), ~ 14.5 m (CH4) (Figure 11a). Whereas, depth estimation by the ERT data are ~ 13.5 m (new PVR), ~ 18 m (ABS Room), ~ 15 m (CH9), ~ 14 m (MB, SP and CH4), ~22 m (old PVR and CH6), ~ 29 m (CH5) ~ 17 m (CH7) respectively (Figure 13e). The calculated depth from these two different datasets show a discrepancy of ~ 2m except at the locations of CH5, CH6 and old PVR. The ERT survey estimates the upper fissured layer depth (~ 9 to 33 meters) of the Choutuppal campus and shows the undulated interface creating compartmentalised aquifers (Nicolas et al., 2019).

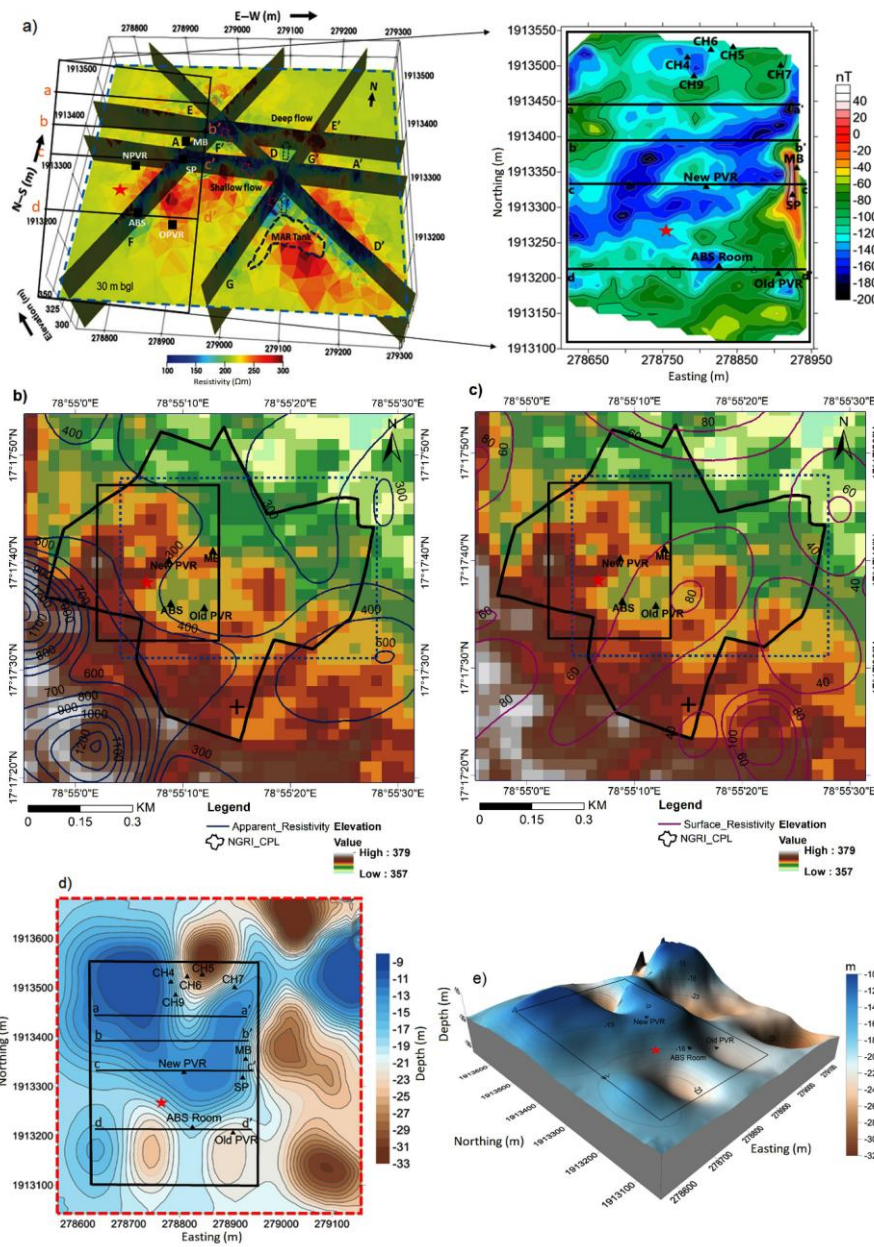
Formatted: Font color: Auto

Formatted: Font color: Auto

Formatted: Font color: Auto

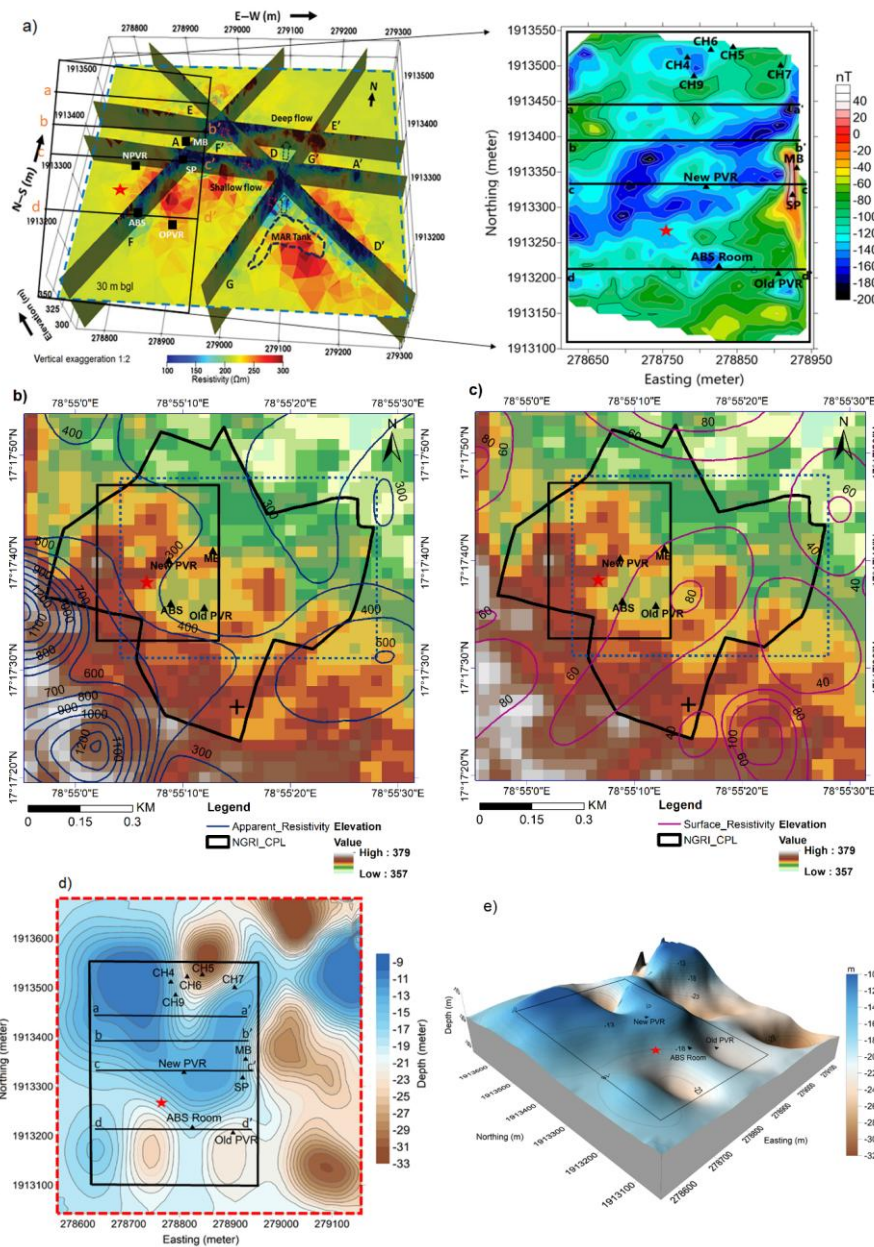
Formatted: Font color: Auto, English (India), Pattern: Clear

Formatted: Font color: Auto, English (India), Pattern: Clear



Formatted: Centered





Formatted: Font: (Default) Arial, Bold

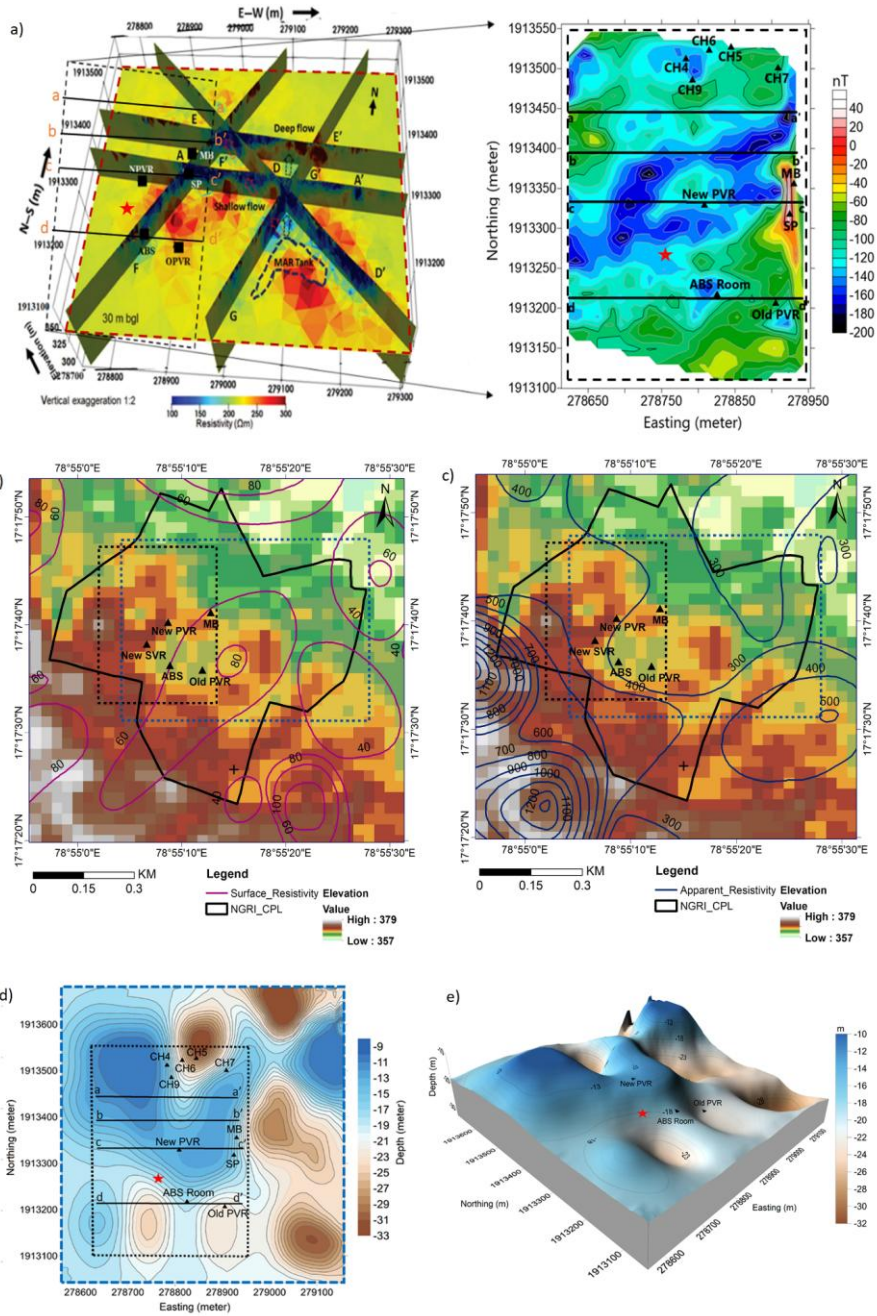


**Figure 13:** a) A resistivity model of the 2019 profiles along AA', DD', EE', FF', and GG' and a depth slice at 30m below ground level (after Maurya et al., 2021), b) surface apparent resistivity, c) surface apparent resistivity superimposed over the topography with lightning strike location (+\* symbol, intensity of 23208 amp. at a distance of 400 m from the MB on 04<sup>th</sup> May, 2022), d) depth estimation of saprolite interface from ERT data (after Nicolas et al., 2019), e) 3D view of saprolite interface ~~from figure 13d~~. The blue and red dotted rectangles represent the areas corresponding to the resistivity model and the saprolite interface, respectively, while the black rectangle highlights the magnetic anomaly region. The blue dotted lines is the area correspond to resistivity model of 2019. Dashed black line shows the magnetic anomaly region.

## 5. Discussion and conclusion: proposed optimal location for SVR

The high resolution magnetic data provide a detailed shallow sub-surface structure at the CPL observatory. The power spectrum result shows two segments at a depth of ~ 12 m and ~1 m corresponding to saprolite and sandy regolith interface. These depths are similar to the previous depth estimated using the drilling data by Dewandel et al., (2006). The inversion results show the depth variation of the saprolite interface ~ 12 to 16 m (Figure 11a) which underestimate with the upper fissured layer depth from the ERT survey (Figure 13d). The obtained interface shows depression in the central region of the map with crests in the outer region and linear variation in depths (Figure 11a). The estimated depths at different locations shows ~ 2 m differences from these two datasets except at the location of CH5, CH6 and old PVR. These discrepancies in the depths estimation may be due to measurements of two different independent physical parameters susceptibility and conductivity. The saprolite interface might be delineate better by the ERT data due to presence of significant resistivity contrast between saprolite and granitic bedrock in the region (Robinson et al., 2008; Gourdol et al., 2021). The tilt depth plot of the anomaly data reflects depth variation from ~ 2 m to 45 m (Figure 10b). The histogram plot confirms the presence of the shallow sources in the depth range of ~ 2 m to 20 m based on the majority of a number of depth

Formatted: Font color: Auto

Formatted: Font color: Auto

Formatted: Font color: Auto

Formatted: Font color: Auto



629 solutions (Figure 10c). These shallow sources are in circular and elongated shapes  
630 which may be residue of igneous intrusion (Gorczyk and Vogt, 2018). At shallow  
631 depths, circular bodies with a magnetic contact source might produce symmetric  
632 anomalies in the magnetic data (Hinze et al., 2013). In contrast, elongated bodies may  
633 produce linear magnetic anomalies that follow the direction of the body as in the  
634 present study.

Formatted: Font color: Auto

635  
636 The sub-surface susceptibility models along the magnetic profiles aa', bb', cc', and dd'  
637 reflect the geometry of sandy regolith, saprolite layer and basement fissured granite  
638 (Figure 12). The saprolite layer shows undulating variation with quiet thick and thin at  
639 different locations along the profiles. These variations illustrate that the saprolite layer  
640 is thin in the region where the anomaly is low and it shows the thickness in the region  
641 where the anomaly is high. The magnetic anomaly shows a large depression of length  
642 ~ 80 m in the profile cc' (Figure 12c) where saprolite layer is absent and this depression  
643 arises due to sandy layer in the model. The 3D cross-sectional resistivity model infers  
644 the presence of high conductive anomalies followed by the moderate conducting  
645 saprolite layer and the low conductive basement rocks (Figure 13a).

Formatted: Font color: Auto

Formatted: Font color: Auto

Formatted: Font color: Auto

646  
647 Figure 13c shows that the apparent resistivity increases laterally outward, indicating  
648 the presence of highly conductive soil layers within the campus. Figures 13c and 13d  
649 show that the apparent resistivity increases laterally away from the campus and shows  
650 the presence of high conductive soil layers inside the campus (Sanker Narayan et al.,  
651 1967). The apparent and surface resistivity demonstrate the linear relationship with  
652 the topography. The comparison between the latest resistivity model (~200  $\Omega$ m  
653 variation) for 2019 profiles (Figure 13a) and the old apparent resistivity (~300  $\Omega$ m

Formatted: Font color: Auto

Formatted: Font color: Auto, English (United States)

Formatted: Font color: Auto

Formatted: Font color: Auto, English (United States),  
Pattern: Clear (White)

variation) plot in 1964 (Figure 13c) shows the resistivity change of ~100 Ωm. This discrepancy may be due to the presence of newly constructed artificial recharge pond which may decrease the resistivity due to its high conductive nature. The thin saprolite layer may be associated with high electrical conductivity, which can result in a low magnetic anomaly, and vice versa. The thin saprolite layer corresponds to high conductivity, which gives low anomaly of the magnetic data and vice versa. Overall, the resistivity variation increases from surface to greater depth. The resistivity model also show that the artificial recharge pond has good subsurface connectivity, helping the groundwater recharge towards the north and northwest directions in the campus (Maurya et al., 2021). The water level started to rise in June-2016 and reached to very shallow depth in channels during December 2017. It is evident that since last half of 2016, the recharge has led to saturation, which transformed the hydrogeological regime of the campus. This may also cause a partial change in the rock magnetism due to water saturation (Csontos et al., 2019) resulting in a decrease in the magnetic anomaly (Figure 4a, 8a). The rainfall of 2017 monsoon combined with the already prevalent saturated conditions led to the flooding of the magnetometer vault. The location of new PVR has advantages as it is away from the water recharge pond, minimal magnetic gradient-anomaly but generation of induced current in the rainy seasons due to presence of conductive environment around the location.

The effect of lightning strikes on the data with increasing distance, intensity and ground conductivity shows that higher intensity strikes has had an impact of the data and instruments.

Formatted: Font color: Auto

Formatted: Font color: Auto

Formatted: English (India)

678 Based on the above it is very crucial to determine the location and configuration where  
679 the installation can avoid the effects of groundwater fluctuations as well as lightning  
680 strikes, based on the nature of subsurface rocks, soil conditions, and their magnetic  
681 variations. The susceptibility model along with conductivity-resistivity information are  
682 used to make a selection of a new SVR site— (78.9185E, 17.2939N) for trial  
683 measurements, indicated by red star in Figures 1, 8, 11, 13. This location is on low  
684 magnetic anomaly of ~ -145 nT (Figure 8a), resistivity ~200 Ωm (Figure 13a),  
685 moderately high ground ~367 m (Figure 13b), and depth of saprolite layer ~ is about  
686 20 m (Figure 13d), conductivity in range of 200 Ωm, magnetic gradient of ~20 nT. A  
687 thicker saprolite layer can enhance the resistive environment and reduce current  
688 propagation. The location's sufficient distance (~ 320 m) from the recharge tank  
689 ensures that water infiltration is unlikely to pose a significant issue. It is proposed that  
690 the pillar will be constructed within a semi-underground vault, in order to minimize the  
691 influence of induced currents during rainy seasons and lightning strikes. Additionally,  
692 the volume surrounding the pillar should be filled using high-resistivity material, such  
693 as Quartzite, to further minimize the likelihood of induced currents during lightning  
694 events or wet conditions.  
695 It is proposed to construct the pillar in a semi underground vault below regolith level,  
696 to avoid additional currents during the rainy season as well as during lightning strikes.  
697 The surrounding area around the pillar should be completely resistive to minimize the  
698 generation of these induced currents. The more thickness of saprolite may create  
699 resistive environment in the region and water may also not create problem due to away  
700 from the recharge tank due to sufficient distance.

Formatted: Font color: Auto

Formatted: Font: Not Bold

Formatted: Font: Not Bold

Formatted: Font: Not Bold

Formatted: Font: Not Bold

Formatted: Font: Not Bold

Formatted: Font: Not Bold

**Acknowledgements:**

We thank the Director, NGRI, for supporting the work; reference no. NGRI/Lib/2025/Pub-35. The authors are thankful to Dr. Subhash Chandra and other colleagues from the ground water department of CSIR-NGRI for providing the bore well water level data and resistivity results. We also thank Dr. Phani Chandrasekhar, [Dr. Rahul Prajapati and Dr. L. Manjula](#) for help towards the repeat surveys.

**Authors' contributions:**

**DD:** Conceptualization, Methodology, Computation and Modeling, Formal analysis, Writing-original draft [and editing](#)

**SY:** Data Processing, Modeling

**KA:** Conceptualization, Validation, Review and final editing

**RM:** Lightning data analysis, maps and figures

**AT:** Lightning data, validation

**Declaration of Competing Interest:**

The authors declare that they have no competing financial interests or personal relationships that could have appeared to influence the work reported in this paper.

**Funding:**

No funding was provided for this work.

## Availability of data and material

The magnetic data associated with this research are available and can be obtained upon the request from corresponding author. The topography data is obtained from the Shuttle Radar Topography Mission (SRTM) Global 30 (<https://earthexplorer.usgs.gov/>). The lightning data can be accessed through the ISRO - National Remote Sensing Centre, Hyderabad ( <https://bhuvan-app1.nrsc.gov.in/lightning/>).

Field Code Changed

Formatted: Font color: Auto

Formatted: Font color: Auto

Field Code Changed

Formatted: Font color: Auto

## References:

Anikiev, D., Götze, H.-J., Plonka, C., et al., 2023. IGMAS+: Interactive Gravity and Magnetic Application System. GFZ Data Services. <https://doi.org/10.5880/GFZ.4.5.IGMAS>.

Field Code Changed

Formatted: Font color: Auto

Formatted: Font color: Auto

Arora K., Chandrashakhar Rao K., Manjula L., et al., 2016. The new magnetic observatory at Choutuppal, Telangana, India. Journal of Indian Geophysical Union, Special volume-2, 67-75.

Arora K., Selles A., Manjula L., et al., 2017. CPL Magnetic Observatory: Groundwater flooding and Relocation requirement. Technical Report No. NGRI-magObs-2017-946.

Chamoli A., Pandey A.K., Dimri V.P., et al., 2011. Crustal configuration of the northwest Himalaya based on modeling of gravity data. Pure and Applied Geophysics 168 (5), 827–844.

Chamoli A., Rana S.K., Dwivedi D., et al., 2023. Crustal structure and fault geometries of the Garhwal Himalaya, India: Insight from new high-resolution gravity data modeling

752 and PSO inversion. Tectonophysics, 859, 229904.  
 753 <https://doi.org/10.1016/j.tecto.2023.229904>.  
 754 [Csontos A., Kónya P., Falus G., et al., 2019. Unstable spatial differences of the](#)  
 755 [geomagnetic elements caused by changing water saturation of a volcanic](#)  
 756 [sediment. Annals of Geophysics, 61\(6\), GM669. https://doi.org/10.4401/ag-7351](#)  
 757  
 758 Dewandel B., Lachassagne P., Wyns R., et al., 2006. A generalized 3-D geological and  
 759 hydrogeological conceptual model of granite aquifers controlled by single or  
 760 multiphase weathering. Journal of Hydrology, 330, 260-284,  
 761 <https://doi.org/10.1016/j.jhydrol.2006.03.026>.  
 762 Dewandel B., Maréchal J.C., Bour O., et al., 2012. Upscaling and regionalizing  
 763 hydraulic conductivity and effective porosity at watershed scale in deeply weathered  
 764 crystalline aquifers. Journal of Hydrology, 416–417, 83-97.  
 765 <https://doi.org/10.1016/j.jhydrol.2011.11.038>.  
 766 Dwivedi D., Chamoli A., Pandey A.K., 2019. Crustal structure and lateral variations  
 767 in Moho beneath the Delhi fold belt, NW India: Insight from gravity data modeling and  
 768 inversion. Physics of the Earth and Planetary Interiors, 297, 106317.  
 769 <https://doi.org/10.1016/j.pepi.2019.106317>.  
 770 Dwivedi D., Chamoli A., 2021. Source Edge Detection of Potential Field Data Using  
 771 Wavelet Decomposition. Pure and Applied Geophysics,  
 772 <https://doi.org/10.1007/s00024-021-02675-5>.  
 773 Dwivedi D., Chamoli A., 2022. Seismotectonics and lineament fabric of Delhi fold belt  
 774 region, India. Journal of Earth System Science, 131, 74.  
 775 <https://doi.org/10.1007/s12040-022-01829-w>.

Formatted: Font color: Auto

Formatted: Font color: Auto

Field Code Changed

Field Code Changed

Formatted: Font color: Auto

Field Code Changed

Formatted: Font color: Auto

Formatted: Font color: Auto

Formatted: Font color: Auto

Field Code Changed

Formatted: Font color: Auto

Formatted: Font color: Auto

Formatted: Font color: Auto

Field Code Changed

Formatted: Font color: Auto

Formatted: Font color: Auto

Field Code Changed

Formatted: Font color: Auto

Formatted: Font color: Auto

776 Gorczyk, W., Vogt, K., 2018. Intrusion of magmatic bodies into the continental crust:  
777 3D numerical models. *Tectonics*, 37, 705–723. <https://doi.org/10.1002/2017TC004738>,  
778 Gourdol, L., Clément, R., Juilleret, J., ~~et al., Pfister, L., and Hissler, C., 2021.~~  
779 Exploring the regolith with electrical resistivity tomography in large-scale surveys:  
780 electrode spacing-related issues and possibility. *Hydrology and Earth System*  
781 *Sciences*, 25, 1785–1812, <https://doi.org/10.5194/hess-25-1785-2021>, 2021.  
782 Guihéneuf N., Boisson A., Bour O., et al., 2014. Groundwater flows in weathered  
783 crystalline rocks: Impact of piezometric variations and depth-dependent fracture  
784 connectivity. *Journal of Hydrology*, 511, 320–334.  
785 <https://doi.org/10.1016/j.jhydrol.2014.01.061>,  
786 Hinze W.J., Von Frese R.R.B., Von Frese R., et al., 2013. Gravity and Magnetic  
787 Exploration: Principles, Practices, and Applications. Cambridge University Press,  
788 Cambridge.  
789 Kumar R., Bansal A. R., Anand S. P., et al., 2018. Mapping of magnetic basement in  
790 Central India from aeromagnetic data for scaling geology. *Geophysical Prospecting*,  
791 66, 226–239.  
792 [Maréchal J. C., Selles A., Dewandel B., et al., 2018. An observatory of groundwater in](#)  
793 [crystalline rock aquifers exposed to a changing environment: Hyderabad, India.](#)  
794 [Vadose Zone Journal](#), 17, 180076, <https://doi.org/10.2136/vzj2018.04.0076>  
795 Maurya V.P., Chandra S., Sonkamble S., et al., 2021. Electrically inferred subsurface  
796 fractures in the crystalline hard rocks of an Experimental Hydrogeological Park,  
797 Southern India. *Geophysics*, 86(5), WB9-WB18, [https://doi.org/10.1190/geo2020-](https://doi.org/10.1190/geo2020-0327.1)  
798 [0327.1](#),  
799 [Maurya V.P., Gupta S.M., Mishra A., et al., 2024. Three dimensional electric field](#)  
800 [vector resistivity imaging for deep subsurface fractures network in heterogeneous](#)

Formatted: Font color: Auto

Field Code Changed

Formatted: Font color: Auto

Formatted: Font color: Auto

Formatted: Font color: Auto

Field Code Changed

Formatted: Font color: Auto

Formatted: Font color: Auto

Field Code Changed

Formatted: Font color: Auto

Field Code Changed

Formatted: Font color: Auto

Formatted: Font color: Auto

801 crystalline rocks, *Geophysical Journal International*, 236 (1), 305–321,  
802 <https://doi.org/10.1093/gji/ggad434>.

803 Miller H. G., Singh V., 1994. Potential field tilt-a new concept for location of potential  
804 field sources. *Journal of Applied Geophysics*, 32, 213–217.

805 Mishra D., Pedersen L.B., 1982. Statistical analysis of potential fields from subsurface  
806 reliefs. *Geoexploration*, 19, 247–265. [https://doi.org/10.1016/0016-7142\(82\)90030-8](https://doi.org/10.1016/0016-7142(82)90030-8).

807 Nicolas M., Bour O., Selles A., et al., 2019. Managed Aquifer Recharge in fractured  
808 crystalline rock aquifers: Impact of horizontal preferential flow on recharge dynamics.  
809 *Journal of Hydrology*, 573, 717–732, <https://doi.org/10.1016/j.jhydrol.2019.04.003>.

810 Parker R., 1973. The rapid calculation of potential anomalies. *Geophysical Journal*  
811 *International*, 31 (4), 447–455, <https://doi.org/10.1111/j.1365-246X.1973.tb06513.x>.

812 Pham L.T., Oksum E., Gómez-Ortiz D., et al., 2020. MagB\_inv: A high performance  
813 Matlab program for estimating the magnetic basement relief by inverting magnetic  
814 anomalies. *Computers & Geosciences*, 134, 104347,  
815 <https://doi.org/10.1016/j.cageo.2019.104347>.

816 Reynolds J., 1997. *An Introduction to Applied and Environmental Geophysics*, Wiley,  
817 Chester, 2nd edition, 710p.

818 Robinso<sub>r</sub>, D. A., Binley<sub>r</sub>, A., Crook<sub>r</sub>, N., et al., 2008. Advancing process-based  
819 watershed hydrological research using near-surface geophysics: A vision for, and  
820 review of, electrical and magnetic geophysical methods, *Hydrological Processes*, 22,  
821 3604–3635, 2008.

822 Salem<sub>r</sub>, A., Williams<sub>r</sub>, S., Fairhead<sub>r</sub>, J., et al., 2007. Tilt-depth method: a simple depth  
823 estimation method using first-order magnetic derivatives. *Leading Edge* 26, 1502–  
824 1505.

Formatted: Font color: Auto

Formatted: Font color: Auto

Formatted: Font color: Auto

Field Code Changed

Field Code Changed

Formatted: Font color: Auto

Formatted: Font color: Auto

Field Code Changed

Formatted: Font color: Auto

Formatted: Font color: Auto

Field Code Changed

Formatted: Font color: Auto

Formatted: Font color: Auto

Field Code Changed

Formatted: Font color: Auto

Formatted: Font color: Auto



825 Sanker Narayan, 1964. Establishment of a magnetic observatory at NGRI. Bull NGRI,  
826 2, 115-122.

827 Sanker Narayan P.V., Ramanujachary K.R., Sarma S.V.S., et al., 1967. Establishment  
828 of a geoelectric observatory by the NGRI, Hyderabad, at Choutuppal, Nalgonda, Bull.  
829 NGRI, 5, 155.

830 Sarma Y.S., Sanker Narayan P.V., Ramanujachary K.R., et al., 1969. Three component  
831 induction magnetometer for recording geomagnetic micropulsations at the Geoelectric  
832 observatory at Choutuppal, Bull. NGRI, 7, 51-65.

833 Spector A., Grant, F.S., 1970. Statistical models for interpreting aeromagnetic data.  
834 Geophysics 35 (2), 293–302.

835 Svendsen, K.L., Davis, W.M., McLean, S.J., Meyers, H. 1990. A report on  
836 geomagnetic observatory operations. NOAA, NGDC, Boulder, Colorado, USA.

837 [Taori A., Suryavanshi A., Pawar S., et al., 2022. Establishment of lightning detection  
838 sensors network in India: generation of essential climate variable and characterization  
839 of cloud-to-ground lightning occurrences. Natural Hazards, 111, 19-32,  
840 <https://doi.org/10.1007/s11069-021-05042-8>](#)

841 [Taori A., Suryavanshi A., Bothale R.V., 2023. Cloud-to-ground lightning occurrences  
842 over India: seasonal and diurnal characteristics deduced with ground-based  
843 lightning detection sensor network \(LDSN\). Natural Hazards, 116, 4037-4049.  
844 <https://doi.org/10.1007/s11069-023-05839-9>](#)

845

846 Telford, W. M., Geldart, L. P., Sheriff, R. E., 1990. Applied Geophysics (2nd ed.).  
847 Cambridge: Cambridge University Press.

Formatted: Font color: Auto

Field Code Changed

Formatted: Font color: Auto

Field Code Changed

Formatted: Font color: Auto

848 Tiwari V.M., Vyghreswara Rao M.B.S., Mishra D.C., et al., 2006. Crustal structure  
849 across Sikkim, NE Himalaya from new gravity and magnetic data. Earth and Planetary  
850 Science Letters, 247, 61-69, <https://doi.org/10.1016/j.epsl.2006.03.037>.

Field Code Changed

Formatted: Font color: Auto

Formatted: Font color: Auto